A MULTIDISCIPLINARY MODELING APPROACH TO ASSESS FACIES-DOLOMITIZATION-POROSITY INTERDEPENDENCE IN A LOWER CRETACEOUS PLATFORM (NORTHERN SPAIN)

MARTA GASPARRINI
IFP Energies nouvelles, 1 & 4 Av. de Bois-Préau, 92852 Rueil-Malmaison, France
e-mail: marta.gasparrini@ifpen.fr

IGNACIO LÓPEZ-CILLA
IGME–Instituto Geológico y Minero de España, Madrid, Spain

SILVIA BLÁZQUEZ-FERNÁNDEZ
IFP Energies nouvelles, Rueil-Malmaison, France and Universidad Complutense, CSIC-UMC, Madrid, Spain

IDOIA ROSALES
IGME–Instituto Geológico y Minero de España, Madrid, Spain

OLIVIER LERAT
IFP Energies nouvelles, Rueil-Malmaison, France

JAVIER MARTÍN-CHIVELET
Universidad Complutense, CSIC—UMC, Madrid, Spain

AND

BRIGITTE DOLIGEZ
IFP Energies nouvelles, Rueil-Malmaison, France

Abstract: An innovative methodology for diagenesis characterization and quantification is presented. It includes different geostatistical modeling workflows applied to a partially dolomitized carbonate platform.

The case study consists of a Lower Cretaceous (upper Aptian) shallow-water carbonate platform from the Basque–Cantabrian basin (northern Spain), in which a widespread burial dolomitization occurs. Previous studies at basin scale suggested that the flow of dolomitizing fluids through the carbonate succession was channeled by regional faults and that subsequently the dolomite distribution was partially controlled by depositional facies and their modifications after early meteoric diagenesis. Here, at reservoir scale, several carbonate facies were differentiated and grouped in five depositional environments. Two depositional sequences corresponding to transgressive–regressive cycles and three stages of the platform evolution were distinguished.

The statistical data treatment indicated that the dolomitization is mainly concentrated in the regressive part of the first sequence, corresponding to the second stage of the platform evolution. The most dolomitized environments are the inner platforms and the shoal. Facies from these shallower/proximal depositional environments were more exposed to early meteoric diagenesis, possibly controlling later dolomitization.

The total macroscopic porosity is directly proportional to the degree of dolomitization: pores are most abundant in fully dolomitized portions of the succession, particularly in the rudist-bearing and grain-dominated facies. Abundant aragonitic shells (rudists, corals), easily leached or recrystallized during early meteoric diagenesis, could justify the higher moldic porosity in these facies.

For geostatistical modeling purposes, several statistical rules were elaborated in order to associate to each depositional environment, in each of the three platform stages, different proportions of dolomitization and related pore abundance. A direct simulation of the distribution of depositional environments, degree of dolomitization, and pore abundance was achieved using a bi-plurigaussian simulation (PGS) algorithm. A nested-PGS algorithm was used to simulate the same parameters independently: dolomite and pore abundance were distributed within each depositional environment, based on the statistical rules previously defined. These simulations allowed three-dimensional (3D) visualization of the original depositional facies and textures affecting the distribution of dolomitization and pore abundance.

Modeling using both bi-PGS and nested simulations accounted for the 3D dolomite body extension: the dolomitized succession is thicker in the north and thins toward the south, in agreement with evidence from mapping of the dolomite geobodies.

Key words: dolomitization, macroporosity, geostatistics, reservoir modeling, Basque–Cantabrian basin, carbonate platform

Characterization and Modeling of Carbonates—Mountjoy Symposium 1
DOI: http://dx.doi.org/10.2110/sepmsp.109.07
SEPM Special Publication No. 109, Copyright © 2017
SEPM (Society for Sedimentary Geology), ISBN 978-56576-352-4, eISBN 978-56576-353-1, p. 130–153.

INTRODUCTION

The quality evolution of carbonate reservoirs may strongly depend on depositional environments and associated facies, with their intrinsic textures and primary mineralogy (Moore 2001, Ali et al. 2010, Morad et al. 2012, Nader 2015). These syn-sedimentary features may induce different early diagenetic evolutions, which in turn are commonly reflected in the distribution of burial diagenetic overprints. In particular, carbonate reservoirs are characterized by significant complexity due to their high reactivity potential, which may induce changes of the initial reservoir properties through various diagenetic processes (i.e., Morrow and MacIlreath 1990, Moore 2001). Dolomitization is a common diagenetic process affecting carbonate reservoirs, and numerous studies have focused on the origin of dolomites in different settings (see Warren [2000] and Machel [2004] for a review). Understanding the petrophysical changes induced in the original lithologies by dolomitization is a crucial topic in hydrocarbon exploration as a result of the possible development of secondary porosity associated with the dolomitization process (i.e., Sun 1995, Saller and Handerson 1998, Morad et al. 2012).

Through the proposed workflows and the use of innovative simulation methods, this study contributes to the need to develop modeling approaches that take into account the interplay between syn-sedimentary features and subsequent diagenetic events, aiming to better predict the overall distribution of reservoir heterogeneities. In order to acquire strong knowledge of the factors governing the heterogeneities in dolomitic reservoirs, it is necessary to characterize their properties at different scales (basin, reservoir, plug, thin section) and with multiple approaches (characterization, quantification, modeling). The geological uncertainty, particularly as it regards petrophysical property distribution in dolomitic reservoirs, could indeed be reduced using geological modeling, which implies systematic treatment of the characterization data. Indeed, through sensitivity analysis, quantitative diagenesis properties can be added to the set of unknown parameters, allowing a better estimate of uncertainties.

Presently, three different numerical approaches are mainly used to simulate diagenesis in geological models: geometry-based, geochemical, or geostatistical approaches (Nader 2017). Geometry-based models provide geometric distribution of heterogeneities as karstification or fracture-related diagenesis. Geochemical modeling uses thermodynamic and kinetic rules to simulate fluid–rock interactions. Finally, geostatistical methods may be used to provide possible distributions of reservoir property heterogeneities. This work will focus on the use of geostatistical methods in workflows consistent with the data properties, interdependencies, proxies, and facies–diagenesis relationships in order to provide pertinent distribution of the petrophysical properties (here macroporosities) within reservoirs.

A wide range of geostatistical methods and algorithms dedicated to lithotype simulations have been developed in the past; they can be ranked from pixel-based (Sequential Gaussian, Truncated Gaussian, Sequential Bayesian Simulations) to object- or process-based models (Journel and Isaaks 1984, Matheron et al. 1987, Srivastava 1993, Galli and Beucher 1997, Armstrong et al. 2011, Strebelle and Cavelius 2014 [among others]). Some of these methods have recently been used to simulate sedimentary facies and associated diagenesis overprints (Labourdette 2007, Pontiggia et al. 2010, Barbier et al. 2011, Doligez et al. 2011, Blázquez-Fernández 2013, Gasparrini et al. 2015, Hamon et al. 2015) and have shown how essential it is to account for quantitative relationships between the depositional lithofacies and the overprinting diagenetic phases (e.g., cements, dissolution, replacements) in order to obtain a consistent distribution of petrophysical properties in the reservoirs. Indeed, one key point for successful reservoir modeling has been demonstrated to be the quantitative integration of the diagenetic overprint in the sedimentary model (Labourdette 2007, Pontiggia et al. 2010).

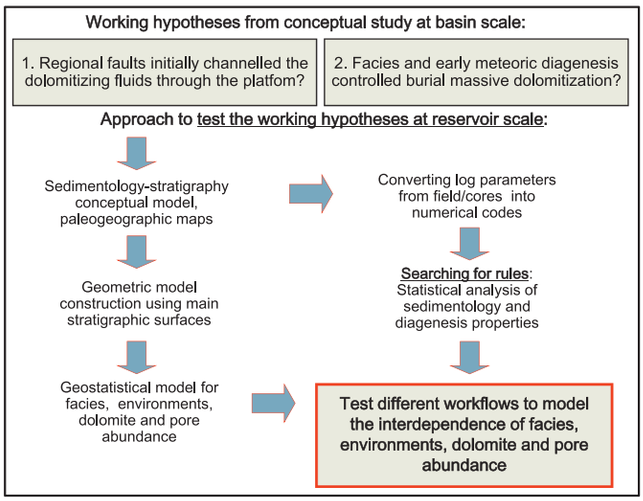

FIG. 1.—Schematic multidisciplinary modeling workflow used.

A Lower Cretaceous (upper Aptian) shallow-water carbonate platform from the northwestern Basque–Cantabrian basin (northern Spain), affected by widespread burial dolomitization, was chosen as the case study. Previous diagenetic studies at basin scale (López-Cilla 2009; López-Cilla et al. 2009, 2013, 2016) suggested that regional faults played a role in channeling the dolomitizing fluids through the platform carbonate pile and that depositional facies and their modifications after early meteoric diagenesis could have further controlled the distribution of burial dolomitization. These working hypotheses formulated at basin scale were tested at the reservoir scale via a complete modeling workflow including field and subsurface data acquisition, statistics of sedimentary–diagenetic properties, and their geostatistical simulation (Fig. 1).

A manageable field-work area was selected in the studied basin, where vertical and lateral relationships between dolomite and original depositional facies can be observed and where shallow subsurface mine cores, provided by the Instituto Geológico y Minero de España (IGME) are available. The aim was to investigate the main controls on the distribution of dolomitization and the effects on the reservoir properties by testing an innovative methodology of diagenesis characterization and quantification, as well as different geostatistical approaches. The entire workflow included several tasks: from field and subsurface data acquisition (stratigraphic logs and facies analysis) to the construction of a geometrical model and from statistical characterization of sedimentary and diagenetic properties (using a log processing tool for well data treatment) to their geostatistical modeling (using advanced geological property grid simulation algorithms).

GEOLOGICAL SETTING

Paleogeography and Tectonics

The study area is located in the northwestern margin of the Basque–Cantabrian basin (Fig. 2), in the Cantabria Community of northern Spain. Geologically, this region has been referred to as the North-Cantabrian basin (Wilmsen 2000, 2005; Martín-Chivelet et al. 2002; Najarro et al. 2007), which formed during the Mesozoic–Early Cenozoic by continental rifting linked to the opening of the Bay of Biscay and the North Atlantic Ocean (Le Pichon and Sibuet 1971, Rat

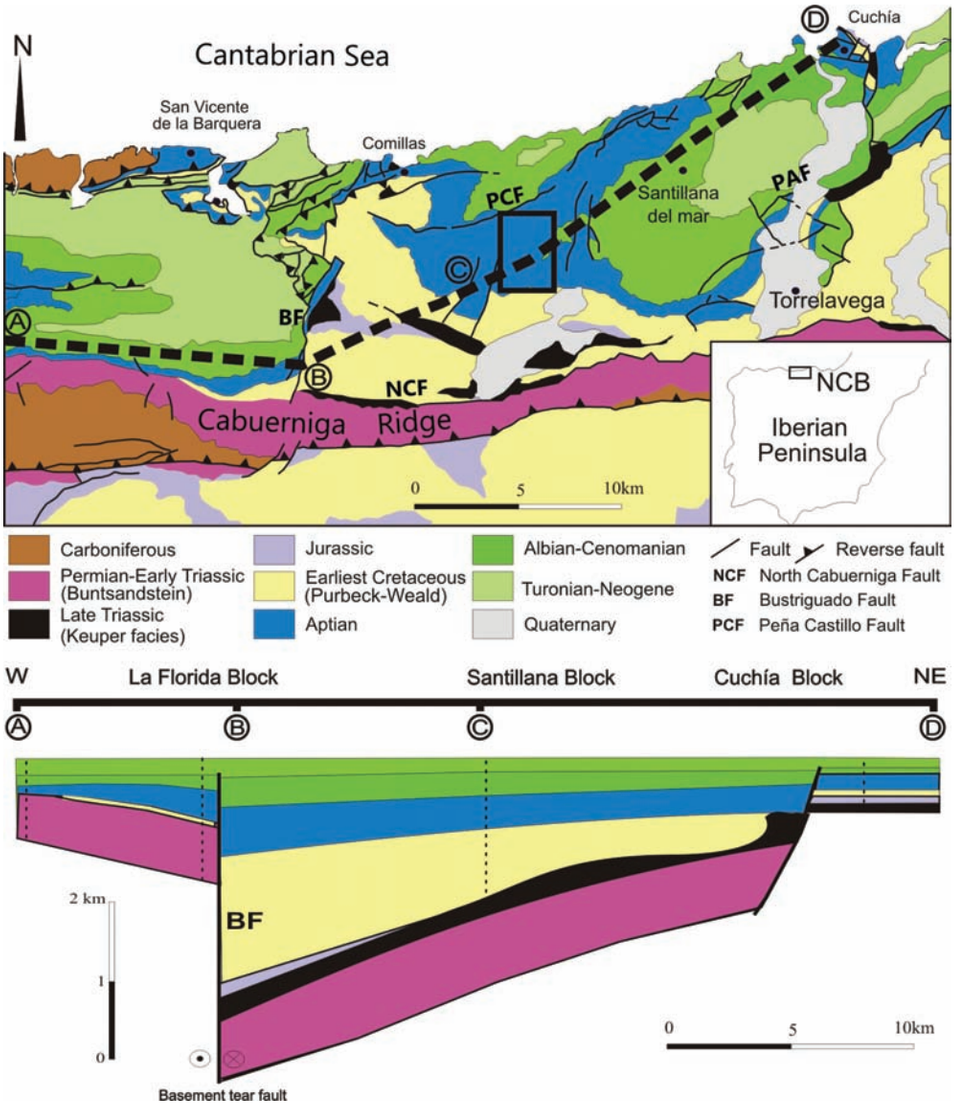

FIG. 2.—Geological map of the North-Cantabrian basin, with the location of the study area represented by a black square (modified after Hines 1985). The line A-B-C-D indicates the trace of the stratigraphic cross section represented below, showing the restored geometry of the basin (after Najarro et al. 2011). BF stands for the Bustriguado fault system.

1988, Malod and Mauffret 1990, Olivet 1996). As a result of the extensional movements, the North-Cantabrian basin underwent strong structural segmentation in a series of horsts and tilted blocks, mainly outlined by syn-sedimentary NE–SW, and E–W oriented faults (Najarro 2015; Fig. 2), which created subbasins and controlled differential subsidence and variations in facies, thicknesses, and stratigraphy over short distances during the Early Cretaceous. These subbasins were filled by syn-rift continental and epicontinental, transitional, and shallow-marine deposits. The studied sections form part of the Lower Cretaceous succession of the Santillana block, a depocentral area flanked by the Bustriguado and Peña Castillo fault systems, with relatively less subsident paleo-highs in the La Florida and Cuchía blocks (Najarro 2015; Fig. 2).

Postrift deposition occurred during the Late Cretaceous and formed a transgressive ramp succession with mainly shallow to outer carbonate platform deposition. Subsequently, basin inversion resulted from convergence between the Iberian and European plates from Santonian to Miocene times. According to the geological data, in the North-Cantabrian basin, the first compressive phases were recorded in the Upper Eocene (Hines 1985, Rat 1988).

General Stratigraphy

As a result of tectonics and eustasy, the North-Cantabrian basin was flooded during the Early Aptian, transforming vast areas formerly characterized by terrigenous deposition (Wealdean facies) into shallow marine environments (Rat 1988). This transgression gave rise to the development of widespread carbonate deposition during the Aptian, resulting in the so-called "Urgonian complex" (Rat 1959, García-Mondéjar 1990). Carbonate rocks belonging to the Urgonian complex

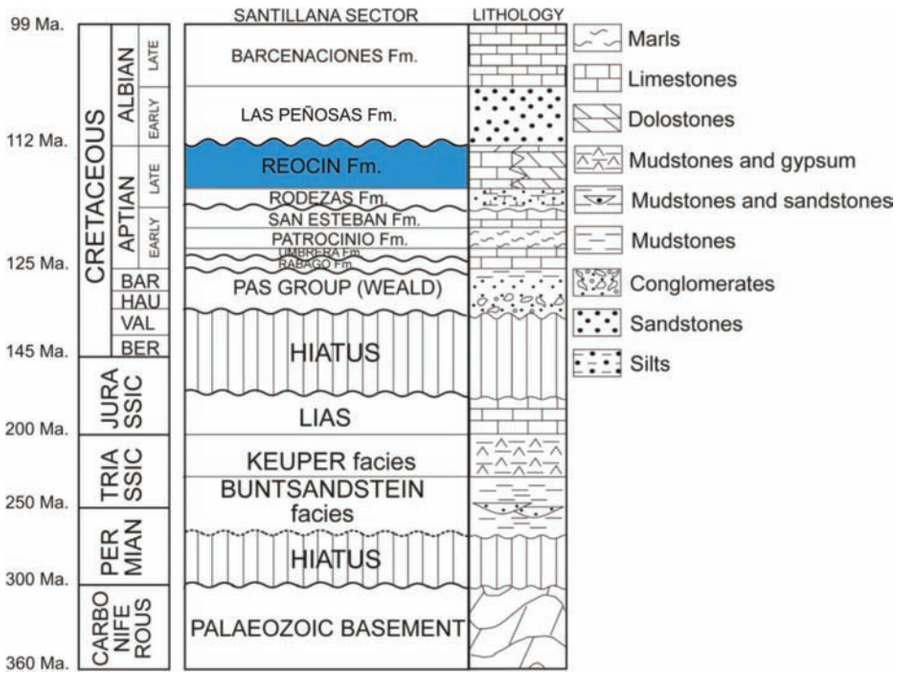

FIG. 3.—Lithostratigraphic framework of the pre-Cenomanian deposits of the Santillana block in the North-Cantabrian basin (modified after Najarro et al. 2011).

consist of shallow-water rudist and coral-dominated limestones with lateral and vertical transitions to continental-transitional siliciclastics and to deeper-water intraplatform basinal marlstones and other basinal sediments (e.g., Rosales 1999).

In the Urgonian complex of the North-Cantabrian basin four main carbonate platform episodes were recorded during the earliest Aptian (Rábago and Umbrera formations [Fms.]; early Bedulian), late Early Aptian (San Esteban Fm., late Bedulian), Late Aptian (Reocín Fm., middle Gargasian–Clansayesian), and Middle–Late Albian (Barcenaciones Fm.) (Hines 1985, Najarro et al. 2011, Najarro 2015, Schlagintweit et al. 2016; Fig. 3). Each of these platform stages was capped by subaerial unconformities followed by transgressive marly and siliciclastic deposits. Major regression in the area during the Early Albian, on the top of the Reocín Fm., resulted in widespread platform exposure, with development of paleokart, and local progradation of deltaic deposits of the Las Peñosas Fm. (Najarro 2015; Fig. 3). Detailed lithological descriptions and age information for these stratigraphic formations are given by previous authors (e.g., García-Mondéjar 1982, Hines 1985, Najarro et al. 2011, Najarro 2015, Schlagintweit et al. 2016).

Dolomite Bodies of the Reocín Fm

This work focuses on the late Aptian Reocín Fm. (7–300 m thick), which consists mainly of shallow-marine wackestone and packstone characterized by the occurrence of rudists, corals, miliolids, orbitolinids, and other benthic foraminifers (e.g., Martín-Chivelet et al. 2002, Najarro et al. 2007, Schlagintweit et al. 2016). The studied sections are located in the depocentral Santillana block (Fig. 4). Here, the Reocín Fm. shows a mean sedimentary thickness of about 210 m, and it is internally subdivided into two carbonate platforms transgressive–regressive sequences (Najarro et al. 2007, Najarro 2015). Only the first sequence and the lower part of the second sequence have been analyzed in this study, which deals with burial, tan to brown-colored, stratabound dolostone bodies, extending laterally for several tens of kilometers. The dolomites preferentially replaced the first carbonate sequence of the Reocín Fm. and particularly its central part (Fig. 4). Previous diagenetic studies at basin scale suggested that the dolomitizing fluids were channeled through the carbonate succession by the main regional NE–SW and E–W oriented faults. Subsequently, a control on the distribution of the burial dolomitization was operated by depositional facies and their modifications after early meteoric diagenesis (López-Cilla 2009; López-Cilla et al. 2009, 2013, 2016). Detailed petrography, geochemistry, and microthermometry suggested a burial genesis for the massive dolomitization (e.g., López-Cilla et al. 2016). The dolomites pervasively replaced matrix, grains, fossils, and early cements. In the study area, however, the dolomitization is partly fabric-retentive (mimetic), preserving the main depositional features, such as textures, grain size, and fossil relics (rudists, orbitolinids, and other bioclasts). At present, these dolostone bodies comprise the main regional aquifer and represent analogues for good-quality oil and gas reservoirs as a result of the presence of various amounts of intercrystalline, moldic, and vuggy pores. Additionally, these pores may host Mississippi Valley–Type Pb–Zn mineral deposits (Reocín Mine District; Bustillo and Ordoñez 1985, Velasco et al. 2003).

DATABASE AND METHODOLOGY

In this study, prior to modeling the spatial distribution of carbonate facies, amount of dolomitization, and reservoir properties, a comprehensive characterization of the studied succession was performed. The methodology included detailed logging and description of field sections and well-cores (both hereafter referred to as "wells"), statistical analyses of the well attributes, and, finally, three-dimensional (3D) geostatistical modeling of the different properties.

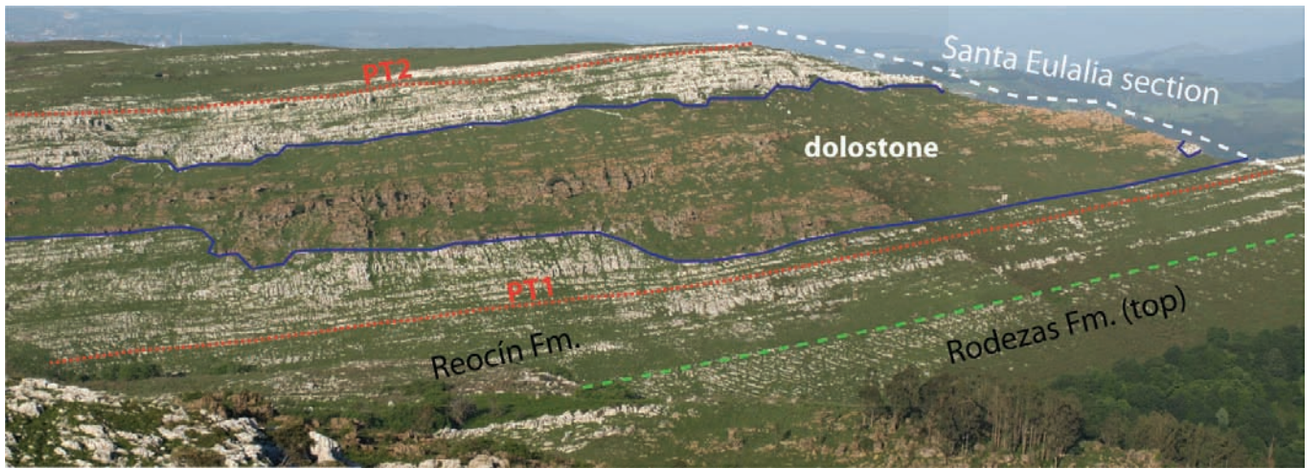

FIG. 4.—Panoramic view of the studied succession of the Reocín Fm. in the Santa Eulalia outcrop (Santillana block). A large, brown-colored stratabound dolomite body can be observed in the central part of the carbonate lithosome. The red lines (PT1 and PT2) represent transgressive surfaces, which have served as correlation lines between the sections analyzed in this study.

Field-work Database

Sedimentological and diagenetic descriptions that constitute the database of this study have been made on six stratigraphic sections logged along the first sequence and the transgressive part of the second sequence of the Reocín Fm. (location map from satellite image in Fig. 5): four outcrop sections (named, from W to E, Duña, Santa Eulalia, Nieves Base, and Nieves Top) and two well-cores (named SC1 and SC6bis) located north of the outcrop area and drilled by the mine company Asturiana del Zinc S.A. The cores are stored in the IGME core repository (Peñarroya).

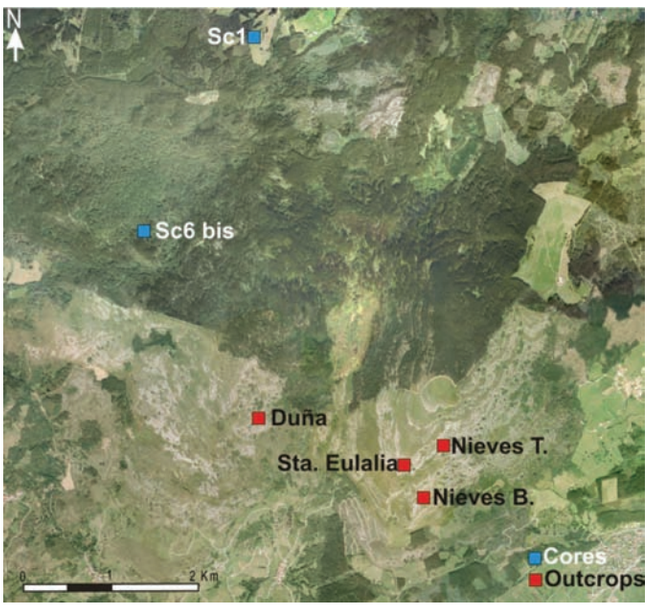

FIG. 5.—Satellite image illustrating the location of the outcrop sections and well-cores investigated in this study.

A classical field and core description methodology for each section has been followed: lithology, textures (sensu Dunham 1962), sedimentary structures, fossil content, and surfaces were recorded. The sections have been logged by including also the description and visual quantification of diagenetic properties on hand specimen fresh cuts (for outcrop sections) and on polished slabs (for core sections). The degree of dolomitization and the dolomite crystal size, as well as the type, size, and abundance of macroscopic pores, were also reported. Diluted HCl and magnification lenses helped in this respect. Intercrystalline, moldic, and vuggy pores were distinguished based on the Choquette and Pray (1970) classification, while fractures (and related porosity) were not reported in the logs. Sedimentological and paleoenvironmental interpretations were based on these field observations. Fifty rock samples were collected with specific focus on facies and diagenetic property changes. Conventional optical petrography was accomplished on thin sections and used for a quality check of the macroscopic visual estimations reported on the logs.

Statistical Analysis

The descriptive properties derived from the macroscopic observations (e.g., facies, dolomite abundance, pore size, etc.) of the six logged sections (here also referred to as "wells") were converted into numerical codes. These codes served as input in the EasyTrace™ software in order to transform the original data set into quantitative and semiquantitative data and to achieve the statistical analysis.

Using EasyTrace™ multivariate statistical analysis on the whole data set has allowed us to highlight the links between depositional facies and the diagenetic properties of interest and their mutual relationships.

Geostatistical Modeling

Geostatistical modeling workflows have been used to simulate sedimentary facies and associated diagenesis overprints (as proposed by Doligez et al. 2009, 2011; Pontiggia et al. 2010; Hamon et al. 2015). The statistical analysis produced quantitative statistical

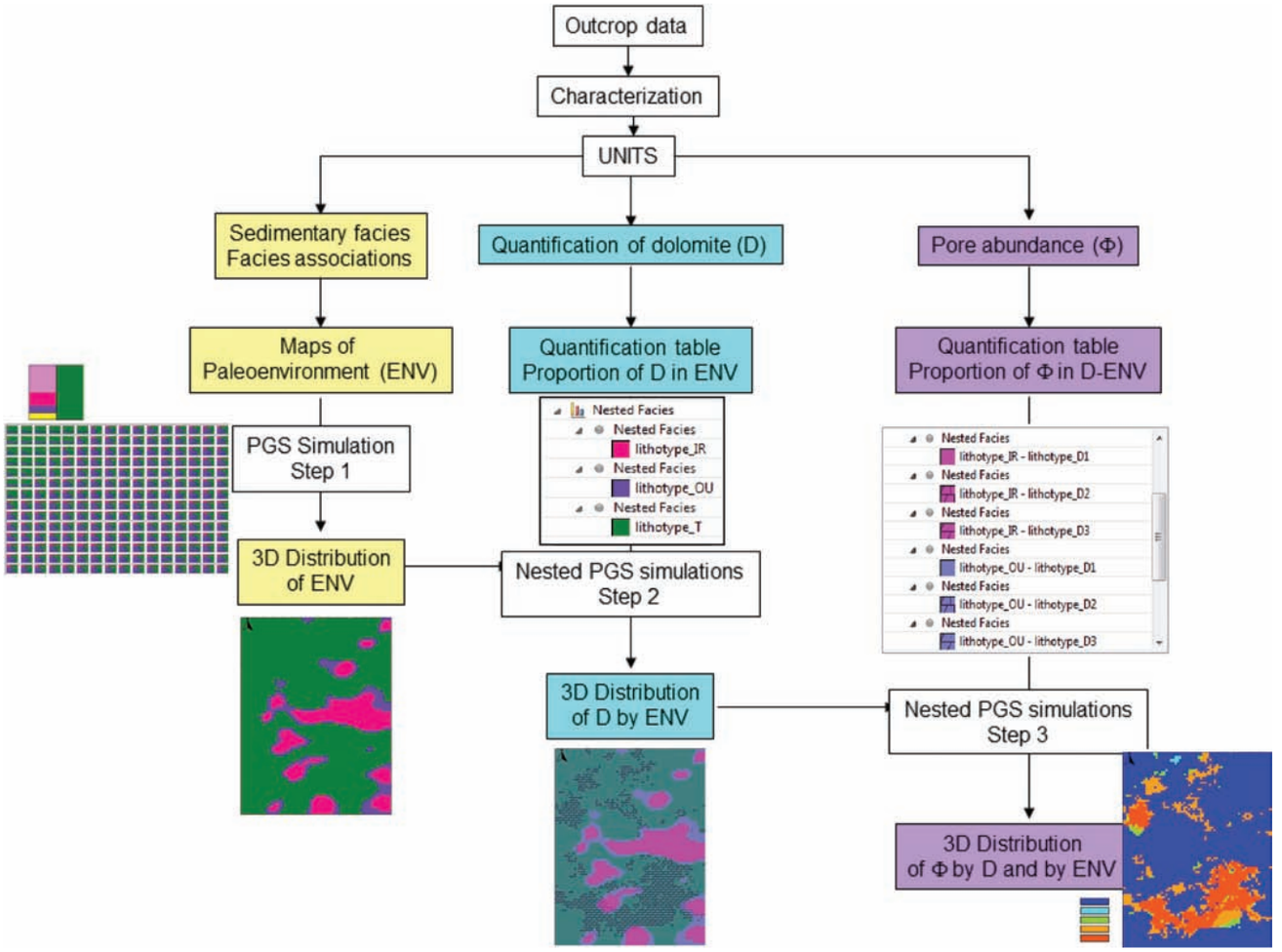

FIG. 6.—Workflow1 or double-nested workflow with the following steps: Step 1—Simulation of the distribution of depositional environments (ENV); Step 2—Nested simulation of the distribution of the amount of dolomite (D in each ENV); Step 3—Nested simulation of the distribution of the pore abundance (Φ) within each couple ENV-D.

distributions of properties within the different depositional facies and environments. These statistics have been used to calibrate parameters for the geostatistical simulations. In this work, we have used two different workflows (using in-house advanced geostatistical property simulation algorithms) to achieve the final goal of producing a numerical model of the studied reservoir with consistent facies, depositional environments, dolomitization, and macroporosity properties.

A first workflow (named "workflow1" or "double-nested workflow"; Fig. 6) was built to better illustrate the distribution of dolomitization and pore abundance in the studied area from simulations of the distribution of depositional environments and diagenetic property quantification. Each consecutive step of the workflow is represented in Figure 6. Since depositional environments, degree of dolomitization (i.e., amount of dolomite), and pore abundance have been proven by the previously undertaken statistical study to be three dependent properties, the workflow integrates three main steps dedicated to the simulation of each of these properties within each of the identified sedimentary units in a double-nested approach, as follows:

- Step 1—Simulation of the distribution of depositional environments using bi-plurigaussian simulation (PGS);
- Step 2—Simulation of the distribution of the amount of dolomite, depending on the depositional environment, using a nested approach (PGS simulation of the amount of dolomite within each depositional environment); and
- Step 3—Simulation of the pore abundance, depending on the amount of dolomite and the depositional environment, using a second step of nested PGS simulation.

A second workflow (named "Workflow2" or "bi-PGS workflow"; Fig. 7) has been tested using combinations of two plurigaussian simulations to co-simulate dependent properties (bi-PGS). The general idea is to generate a model of the depositional environment distribution that can be controlled by the conceptual geological knowledge using a PGS method. The diagenetic imprint distribution (degree of dolomitization in this case) is generated using the

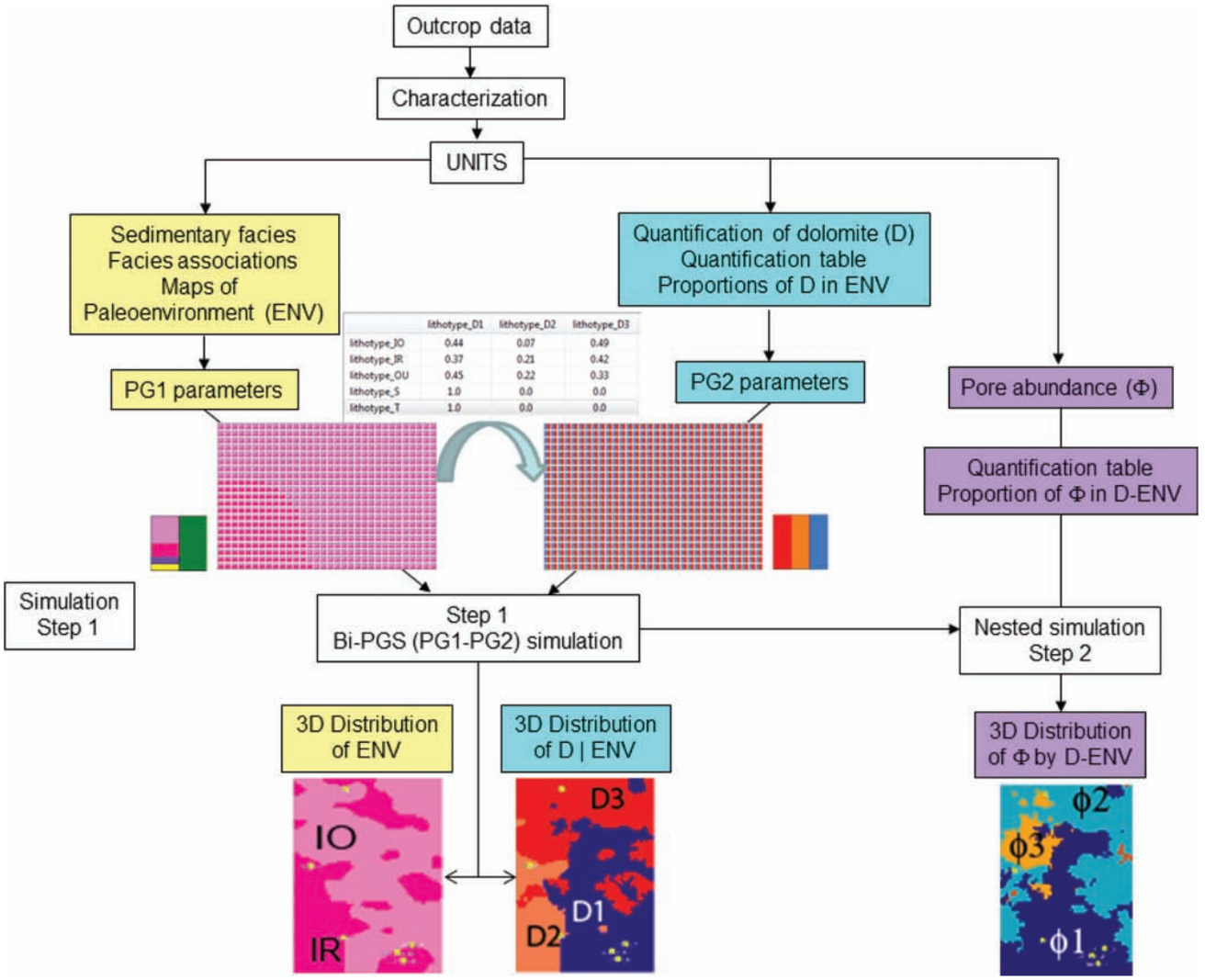

	lithotype_D1	lithotype_D2	lithotype_D3
lithotype_IO	0.44	0.07	0.49
lithotype_IR	0.37	0.21	0.42
lithotype_OU	0.45	0.22	0.33
lithotype_S	1.0	0.0	0.0
lithotype_T	1.0	0.0	0.0

FIG. 7.—Workflow2 or bi-PGS-nested workflow with the following steps: Step 1—Co-simulation of the distribution of environments (ENV) and amount of dolomite (D) using the new bi-PGS method; Step 2—Nested simulation of the distribution of pore abundance (Φ) within each couple ENV-D.

quantified proportions between the initial rock textures and their subsequent alteration (diagenesis) and a second PGS simulation, the parameters of which are conditioned by the association rules between depositional environments and diagenetic properties of interest. Using this second plurigaussian simulation means that continuity in the diagenetic property from one cell to another can be obtained, even if the sedimentary facies changes between these cells (which would not be possible with a nested approach; Doligez et al. 2011).

RESULTS OF SEDIMENTOLOGY AND STRATIGRAPHY

Based on the information collected along the six detailed sedimentological logs investigated, a facies analysis study was performed, different conceptual depositional models were established, and a sequential correlation was accomplished.

Facies Analysis

Sixteen depositional lithofacies plus two diagenetic lithofacies (excluding dolomitization) have been distinguished throughout the logged sections of the Reocín Fm. (18 lithofacies in total; see Table 1). The 16 depositional lithofacies have been defined based on macroscopic observations of lithology, texture, allochems, paleontological constituents, and sedimentary structures, along with additional information obtained from microfacies analysis on thin sections.

Where the studied lithologies are dolomitized, the identification of the original depositional lithofacies is more complex but is still made possible by the relatively good preservation of original bedding, depositional structures and textures, and specific fossil components or molds. Thus, according to the preserved fabrics, six dolo-textures have been distinguished: dolo-mudstone, dolo-wackestone, dolo-floatstone, dolo-packstone, dolo-grainstone, and dolo-rudstone (Fig. 8). For instance, the dolo-rudstone is the dolomitized equivalent of

TABLE 1.—Summary of the 18 lithofacies (depositional and diagenetic) identified from outcrops and cores and grouped according to the depositional environment of provenance. The table also includes sedimentology and paleoecology information for each of these facies.

Facies		Texture	Biotic content		Other components	Sedimentary features and bioturbation	Depositional environment	
			Dominant	Accessories				
GS1	Fine-grained peloidal packstone.	Grain-supported.	Peloids.	Sponge spicules and echinoderm debris.	Small benthic foraminifera.	Well-sorted fine to very fine packstone.	Low energy, open-marine circalittoral zone.	Outer platform
GS2	Orbitolinid packstone.	Grain-supported.	Orbitolinids.	Fine- grained debris of brachiopods, bivalves, echinoderms, inoceramids and benthic foraminifera.	Quartz silt.	Occasional wavy lamination.	Open sea with moderate energy, circalittoral zone.	
MS5	Marls and nodular limestones.	Mud-supported.	Orbitolinids.	Massive corals.		Marls and nodular limestones with orbitolinids. *Thalassinoides.*	Outer platform, upper circalittoral zone.	
GS3	Bio- and intraclastic grainstone.	Grain-supported.	Echinoderm plates.	Textularids, bivalve fragments (rudists, oysters), miliolids, bryozoans, fragmented orbitolinids, remains of brachiopods, crinoid ossicles, massive coral fragments.	Micritized grains, limestone intraclats, sandstone lithoclast and quartz sand grains.	Medium to coarse, moderately sorted and rounded to sub-rounded grains. Wavy and cross stratification.	High-energy open platform. Transition circalittoral-infralittoral zone, at or near the fair-weather wave base.	Marginal shoal complexes
GS4	Peloidal packstone-grainstone.	Grain-supported.	Peloids and micritized grains.	Miliolids, textularids, lituolids, gastropods (nerineids), debris of rudists, orbitolinids, corals, calcareous sponges, echinoid.			Transition circalittoral to infralittoral zones. Locally in open inner platform.	Transitional outer to inner platform
MS4	Coral wackestone.	Mud-supported.	Massive and tabular corals.	Bioclasts include coral fragments, echinoderm debris, pelecipods, calcareous sponges and orbitolinids.		Bioclastic wackestone and packstone colonized by massive and tabular corals.	Open marine, middle platform.	
GS5	Miliolid-rich packstone to grainstone.	Grain-supported.	Miliolids.	Benthic foraminifera (lituolids, textularids, orbitolinids), green algae, bioclasts (echinoderm, gastropods, rudist).	Micritized grains and peloids.		External inner platform. Normal salinity. Lower to intermediate infralittoral.	Inner open platform
GS6	Coral packstone	Grain-supported	Fragmented and whole branching corals.	Benthic foraminifera (textularids, miliolids), gastropods, *Lithocodium-Bacinella* (lumps and encrusting masses). Bioherms of branching corals.		Fine-grained packstone to grainstone, locally wackestone.	Shallow subtidal platform, infralittoral. Transgressive facies.	
GS7	*Lithocodium-Bacinella* packstone to grainstone.	Grain-supported	*Lithocodium-Bacinella*.	Coral and rudist fragments.	Micritized grains and peloids.	*Lithocodium-Bacinella* lumps and ameboidal oncoids floating in skeletal packstone to grainstone.	Moderate energy. External inner platform, infralittoral. Transgressive facies.	
GS8	*Lithocodium-Bacinella* oncoidal rudstone.	Grain-supported	*Lithocodium-Bacinella* oncoids	Small requieniid rudists	Micritized grains.	Rudstone of centimetric, sub-rounded *Lithocodium-Bacinella* oncoids in wackestone to packstone matrix.	Inner platform. Upper infralittoral to supralittoral. Most regressive and early transgressive facies.	
MS1	Foraminiferal wacke-mudstone.	Mud-supported.	Miliolid and benthic foraminifera.	Requieniid rudists and/or small gastropods or tiny bivalves.	Peloids and micritized grains.	Wavy to nodular wackestone to mudstone. Bioturbated	Low energy, muddy inner platform, infralittoral zone.	Inner restricted to lagoonal platform.
MS2	Bio- and peloidal wackestone.	Mud-supported.		Fragments of oysters, rudists, branching corals, calcareous algae. Miliolids, orbitolinids, textularids. Occasionally large requieniids, nerineids, *Lithocodium-Bacinella* fabrics, echinoderm debris.	Peloids and micritized grains.		Low energy. Middle part for the inner platform, infralittoral zone.	
MS3	Rudist and *Lithocodium-Bacinella* floatstone.	Mud-supported.	Rudists, *Lithocodium-Bacinella*.	Cyanophyceans, dasycladaceans, miliolids, small benthic foraminifera, small gastropods and bioclasts.	Micritized grains.	Articulated rudists and *Lithocodium-Bacinella* thrombolitic fabrics in a matrix of clotted to dense micrite.	Infralittoral, subtidal environment. Protected lagoon in the inner part of the inner platform.	
MS6	Gastropod wacke-mudstone.	Mud-supported.	Gastropods.				Restricted inner platform-lagoon.	
BS1	*Lithocodium-Bacinella* boundstone.	Boundstone.	*Lithocodium-Bacinella* thrombolites.			Mudstone with irregular masses of *Lithocodium-Bacinella* with thrombolitic fabrics.	Protected lagoon. Inner part of the inner platform. Infralittoral zone.	
BS2	Rudist boundstone.	Boundstone.	Requieniid, polyconitid and radiolitid rudists.	Bioclasts, miliolids, textularids, orbitolinids.	Peloids and micritized grains.	Banks 1 to several meters thick and tens to hundred meters long. Wackestone-packstone matrix.	Infralittoral zone. External part or the inner platform.	
H	Hydraulic breccias.	Diagenetic.	Non-observed.	Non-observed.	Non-observed.	Non-observed.	Non-observed.	Non-observed
D	Dedolomite.	Diagenetic.	Non-observed.	Non-observed.	Non-observed.	Non-observed.	Non-observed.	

the rudist–boundstone facies. In the cores, two additional diagenetic lithofacies have been distinguished, where the original limestone texture could not be recognized: hydraulic breccias and dedolomite (H and D in Table 1). The latter includes strongly dedolomitized and weathered lithologies that could not be attributed to a specific depositional lithofacies. These two diagenetic lithofacies (hydraulic breccias and dedolomite) do not have any relationship to depositional lithofacies, and they have not been modeled. The limestone facies and their dolomitized equivalents have been grouped into four main classes based on the depositional or diagenetic fabrics: grain-supported (GS), mud-supported (MS), boundstone (BS), and diagenetic facies (D, H). The facies analysis information is summarized in Table 1 and Figure 8.

Facies Associations and Depositional Environments

The 16 depositional lithofacies identified have been grouped into five facies associations based on genetic facies relationships and depositional environments, as follows: outer platform (OP), transitional outer–inner platform (T), shoal (S), inner open platform (IO), and inner restricted platform (IR). The main characteristics of the lithofacies types comprising these facies associations are summarized in Table 1 and Figure 9.

Outer Platform (OP): Bioturbated marlstones and argillaceous nodular limestones (MS-5), laminated, fine grained peloidal–foraminiferal packstone (GS-1), orbitolinid-rich packstone (GS-2), and coral wackestone (MS-4) dominate this facies association. The most common skeletal components are orbitolinids, small benthic foraminifers, echinoderms, sponge spicules, oysters, and massive corals. This facies association is interpreted as being deposited in outer parts of the platform under low-energy hydrodynamic conditions. The presence of corals suggests water depth within the photic zone.

Transitional Outer–Inner Platform (T): This facies association consists of medium to fine grained packstone and grainstone with peloids and micritized grains, bioclasts, miliolids, orbitolinids, small benthic foraminifers, coral fragments, and sponges (GS-4). It is interpreted as being deposited under moderate-energy hydrodynamic

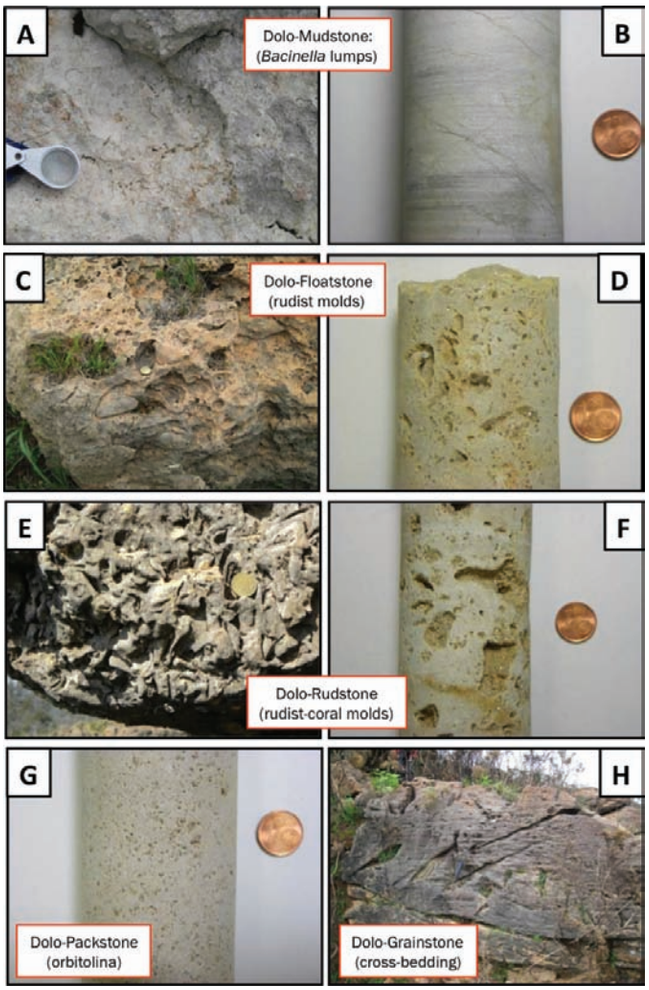

FIG. 8.—Textures identified from field and core observations. **A, B)** Dolomudstone in outcrop and core views, respectively; **C, D)** Dolo-floatstone, with rudist molds, in outcrop and core views, respectively; **E, F)** Dolo-rudstone with large rudist molds, in outcrop and core samples, respectively; **G)** Dolo-packstone, with orbitolinid molds, in a core sample; **H)** Dolo-grainstone in outcrop view with cross bedding.

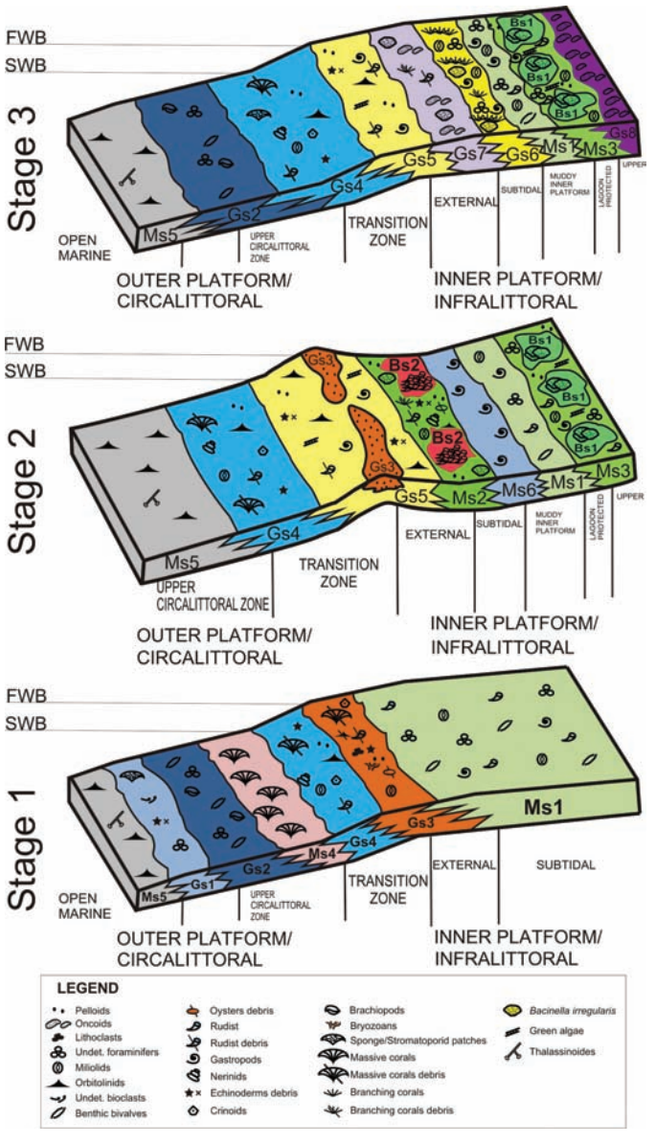

FIG. 9.—Conceptual depositional models of the three stages of the platform evolution. Stage 1 is a transgressive, mainly grain-dominated open platform. Stage 2 is a regressive platform with inner restricted and shoal marginal environments. Stage 3 is characterized by transgressive open platform facies. Lithofacies colors and codes as in Table 1.

conditions, in an open environment at the transition between the outer and the inner platform.

Shoal (S): It consists of wavy and cross-laminated, medium- to coarse-grained, bioclastic and intraclastic grainstone (GS-3). The main components include intraclasts, echinoderm debris, micritized grains, benthic foraminifers, bryozoans, crinoidal ossicles, bivalve and coral fragments, and quartz sand grains. The sedimentary structures and textures suggest a high-energy hydrodynamic environment above or close to the fair-weather wave base, most likely representing sand shoal complexes, with sand waves and sand channels, deposited in a shallow subtidal platform margin setting.

Inner Open Platform (IO): It is mainly composed of packstone and grainstone with miliolids (GS-5), corals (GS-6), *Lithocodium–Bacinella* lumps (GS-7), and rudstone of *Lithocodium–Bacinella* oncoids (GS-8). Frequent allochems in these lithofacies are branching corals (fragmented or in live position), miliolids, benthic foraminifers, and green codiacean and dasycladalean algae, as well as lumps and ameboidal oncoids of the problematic *Lithocodium–Bacinella* calcifying cyanobacteria (Riding 1991). These lithofacies are stacked aggradationally at the upper part of the studied succession.

The presence of branching corals and green algae suggests shallow platform environments under normal-salinity seawater. The microbial *Lithocodium–Bacinella* facies have been reported in a wide range of water depth, from deep subtidal to shallowest subtidal

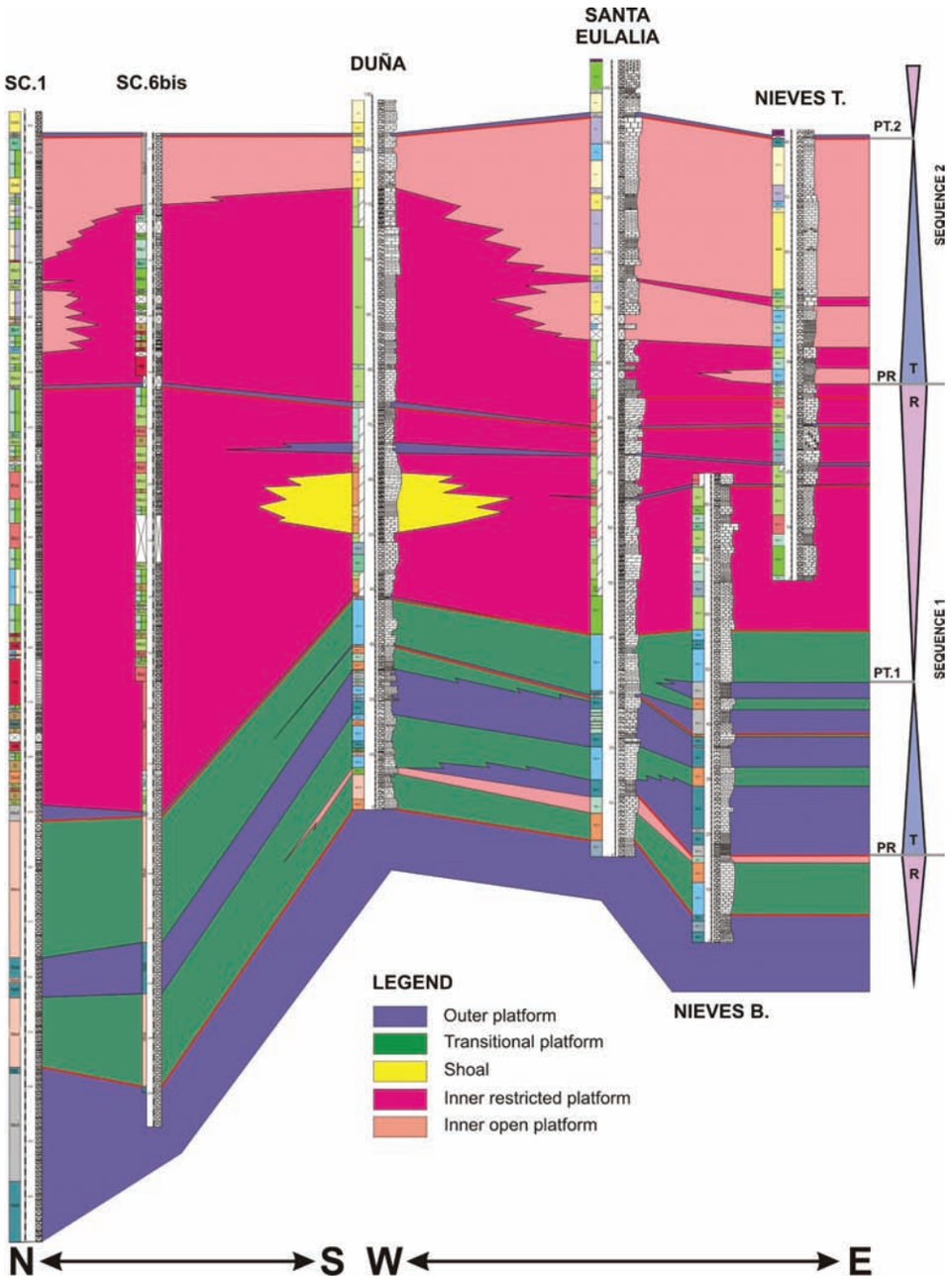

FIG. 10.—Correlation diagram of the logged sections with interpretation of lateral and vertical distribution of depositional environments and depositional (T–R) sequences: transgressive (T), regressive (R), peak transgression (PT), peak regression (PR). Lithofacies colors and codes as in Table 1.

and even intertidal conditions, with maximum depth limited to the photic zone (Neuweiler and Reitner 1992, Rameil et al. 2010). Their proliferation has been associated with either shallow-water platform environments with open marine conditions (Hamdan and Alsharhan 1991) or open lagoonal environments under specific paleoceanographic conditions of high trophic levels (Immenhauser et al. 2005, Huck et al. 2010, Bover-Arnal et al. 2011). Here, according to the biotic assemblage, this facies association is interpreted as being deposited in inner open platform environments.

Inner Restricted Platform (IR): It is formed predominantly by muddy lithofacies that include foraminiferal wackestone–mudstone (MS-1), bio- and peloidal wackestone (MS-2), rudist and *Lithocodium–Bacinella* floatstone (MS-3), *Lithocodium–Bacinella* boundstone (BS-1), and rudist boundstone (BS-2). The rudist-dominated

floatstone and boundstone are volumetrically the most representative lithofacies types. Rudist boundstone banks are one to several meters thick and tens to hundreds of meters long, with the rudists bound together mainly in life position. Rudist types include requieniids (dominant), polyconitids, and radiolitids. The muddy carbonate factory and the occurrence of requieniids mainly in life position suggest deposition in a low-energy, muddy inner platform or lagoon with restricted water circulation (e.g., Masse and Philip 1981, Masse and Fenerci-Masse 2011).

Lithofacies Trends and Sequences

Based on vertical-deepening and shallowing-upward trends of lithofacies and identification of some key stratigraphic surfaces, two transgressive–regressive (T–R) sequences (Vail et al. 1991, Embry 1993) have been recognized for the studied succession of the Reocín Fm. (Fig. 10). Below these two sequences (Sequences 1 and 2; Fig. 10), the most regressive part of an older depositional sequence, corresponding to the transition between the Rodezas and Reocín Fms., can also be observed.

Sequence 1 is approximately 85 m thick. It has a transgressive part that measures approximately 31 m, composed mainly of marlstone and marly limestone (MS-5) and orbitolinid packstone (GS-2), with sparse interbedded meter-scale intercalations of bioclastic–intraclastic grainstone (GS-3). The peak transgression is placed on the top of the thickest marly interval (PT1 in Figs. 4, 10). The regressive part is about 54 m thick and is characterized by rudist-bearing lithofacies (MS-3, BS-2) accompanied by nerineid gastropod, peloidal, and foraminiferal wackestone (MS-1, MS-2, MS-6) and boundstone of *Lithocodium–Bacinella* masses (BS-1).

As a result of the lack of evidence for subaerial exposure, the boundary between Sequences 1 and 2 (PR in Fig. 10) is expressed by a change from inner-platform rudist-dominated facies to open platform orbitolinid-rich marlstones and coral and *Lithocodium–Bacinella* limestones.

Sequence 2 is at least 60 m thick, and only the transgressive part of the cycle is studied here (Fig. 10). These transgressive deposits are characterized by the occurrence of aggradational, grain-dominated deposits with extensive development of corals and *Lithocodium–Bacinella* lumps and oncoids (GS-5, GS-6, GS-7, GS-8). The maximum flooding zone (PT2 in Figs. 4, 10) has been placed within a marly bed with orbitolinids that constitutes the upper datum for correlation between the studied sections.

Three stages of platform evolution have been differentiated (Blázquez-Fernández 2013; Fig. 9). Stage 1 occurs during the transgressive phase of Sequence 1. It is characterized by T and OP environments dominated by marly and grain-supported lithofacies. Stage 2 characterizes the regressive phase of Sequence 1. It is characterized by IR or lagoonal environments with proliferation of rudist-bearing facies, and grain-dominated S environment toward marginal settings. Stage 3 occurred during the transgressive phase of Sequence 2. It is dominated by IO environments, deposited in a transgressive setting, characterized by grain-supported textures with coral and *Lithocodium–Bacinella* lumps (Fig. 10).

Using the whole facies analysis information, five paleoenvironmental maps were constructed: two for Stage 1, two for Stage 2, and one for Stage 3 (Blázquez-Fernández 2013). They were used to better constrain the modeling of the geological properties (see next sections).

RESULTS OF STATISTICAL ANALYSIS

The statistical analysis was accomplished to highlight relationships and interdependence between the sedimentological and diagenetic parameters described during field-work: principally facies, depositional environments, dolomite abundance, and pore abundance. In order to enter the information from the field-work data set into the EasyTrace™ software the classes established for each parameter were expressed using numerical codes (Table 2).

TABLE 2.—Tables summarizing the codes attributed to each property examined for statistics.

Facies	Code
GS1	1
GS2	2
GS3	3
GS4	4
GS5	5
GS6	6
GS7	7
GS8	8
MS1	9
MS2	10
MS3	11
MS4	12
MS5	13
MS6	14
BS1	15
BS2	16
MS1-2	17
HB	18
D	19
GS5-7	20
GS4-5	21

Environments	Code
Outer Platform (OP)	1
Transitional (T)	2
Inner Restricted (IR)	3
Inner Open (IO)	4
Shoal (S)	5

Pore abundance	Code
Absent	1
Rare	2
Rare to Commun	3
Rare and Abundant	4
Common	5
Common to Abundant	6
Abundant	7

Facies Groups	Code
Muddy facies	1
Fine grained facies	2
Medium-coarse grained facies	3
Rudist-rich or bearing facies	4
Diagenetic (breccia, dedolomite)	5

Dolo quantity	Code	Model
nothing	1	D1
<10 %	2	
10-25 %	3	D2
25-50%	4	
50-75%	5	
75-100%	6	D3

The original limestone lithofacies (Table 1) and their dolomitized counterparts have been distinguished for the statistical treatment in 21 facies classes (Table 2). These facies classes were grouped into five broader classes (referred to as "Facies Groups" in the figures and tables), mainly on the basis of the texture, grains size, and dominant bioclast. These are muddy facies (code 1), fine grained facies (code 2), medium-coarse grained facies (code 3), rudist-rich (or bearing) facies (code 4), and diagenetic facies (code 5).

The different depositional environments (referred to as "Environment" in the figures and tables) were coded as follows (Table 2): OP (code 1), T (code 2), IR (code 3), IO (code 4), and S (code 5).

For the amount of dolomite (referred to as "Dolo Quantity" in the figures and tables), six classes were distinguished (Table 2): 0% of dolomite (code 1), less than 10% of dolomite (code 2), dolomite in the range of 10 to 25% (code 3), dolomite between 25 and 50% (code 4), dolomite in the range of 50 to 75% (code 5), and dolomite between 75 and 100% (code 6). For geostatistical modeling purposes these initial six classes were later grouped in three broader classes: undolomitized lithologies (named D1) with dolomite in the range of 0 to 10% (including codes 1 and 2); partially dolomitized lithologies (named D2) with dolomite in the range of 10 to 75% (including codes 3, 4, and 5); and fully dolomitized lithologies (named D3) with dolomite in the range of 75 to 100% (including code 6).

The abundance of pores (referred to as "Pore Abundance" in the figures and tables) was coded as follows (Table 2): absent pores (code 1), rare pores (code 2), rare to common pores (code 3), bimodal rare and abundant pores (code 4), common pores (code 5), common to abundant pores (code 6), and abundant pores (code 7). Code 4 (rarely observed) refers to samples that contain two different types of porosity (e.g., moldic and intercrystalline or moldic and vuggy), being, respectively, rare and abundant. For geostatistical purposes, these seven initial classes were later grouped into five broader classes by merging together classes 3 and 4 and classes 5 and 6.

In the following histograms, representing the results of the statistical treatment, the values reported as "777" correspond to undefined, but not null, values in the log data set. This is because at the same well depth information is not available for all properties. These values were not taken into account when computing statistics (mean, standard deviation, etc.).

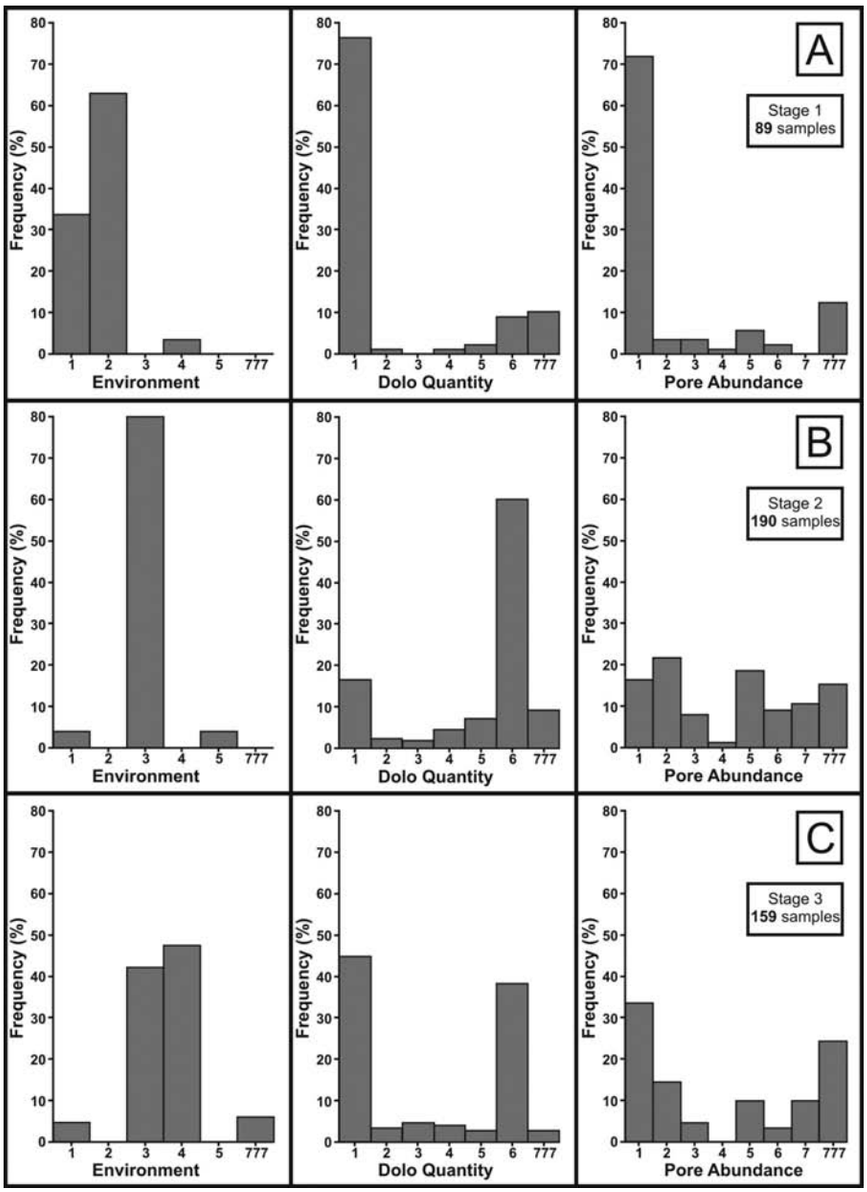

FIG. 11.—Frequency distribution of the "Environment," "Dolo Quantity," and "Pore Abundance" for the three stages of platform evolution. **A)** Stage 1 (89 samples). **B)** Stage 2 (190 samples). **C)** Stage 3 (159 samples). See Table 2 for the code explanation.

In terms of dolomite abundance ("Dolo Quantity"), the analysis on the complete succession, including the three platform stages, shows that 44% of the total rock volume is fully dolomitized (75–100% of dolomite; D3), 45% is not dolomitized or poorly dolomitized (<10% of dolomite; D1), and 11% is partially dolomitized (10–75% of dolomite; D2).

In terms of pore abundance ("Pore Abundance") in the whole succession, 60% of the total rock volume displays pores falling in the "absent" and "rare" classes (codes 1 and 2) and 22% is given by pores in the "rare to common" and "common" classes (codes 3 and 5), whereas only 17% of the rock volume displays pores in the "common to abundant" and "abundant" classes (codes 6 and 7). Class 4 is poorly represented in the succession.

With regard to the relative abundance of depositional environments ("Environment") in the whole succession, the IR is the best represented, although some differences are highlighted when observing the facies distribution for each of the three platform stages individually (Fig. 11). Moreover, the distribution of depositional environments through the different stages of the platform is also reflected in different proportions of dolomitization and associated macroscopic pores. Indeed, in Stage 1 (Fig. 11A), which is dominated by T (code 2) and OP (code 1) environments, the fully dolomitized rock volume (code 6) represents less than 10%, and the pores are dominantly (>70%) absent. In Stage 2 (Fig. 11B), the dominant environment is the IR (code 3), with appearance of minor S (code 5). This is the most dolomitized of the three stages, in which the fully

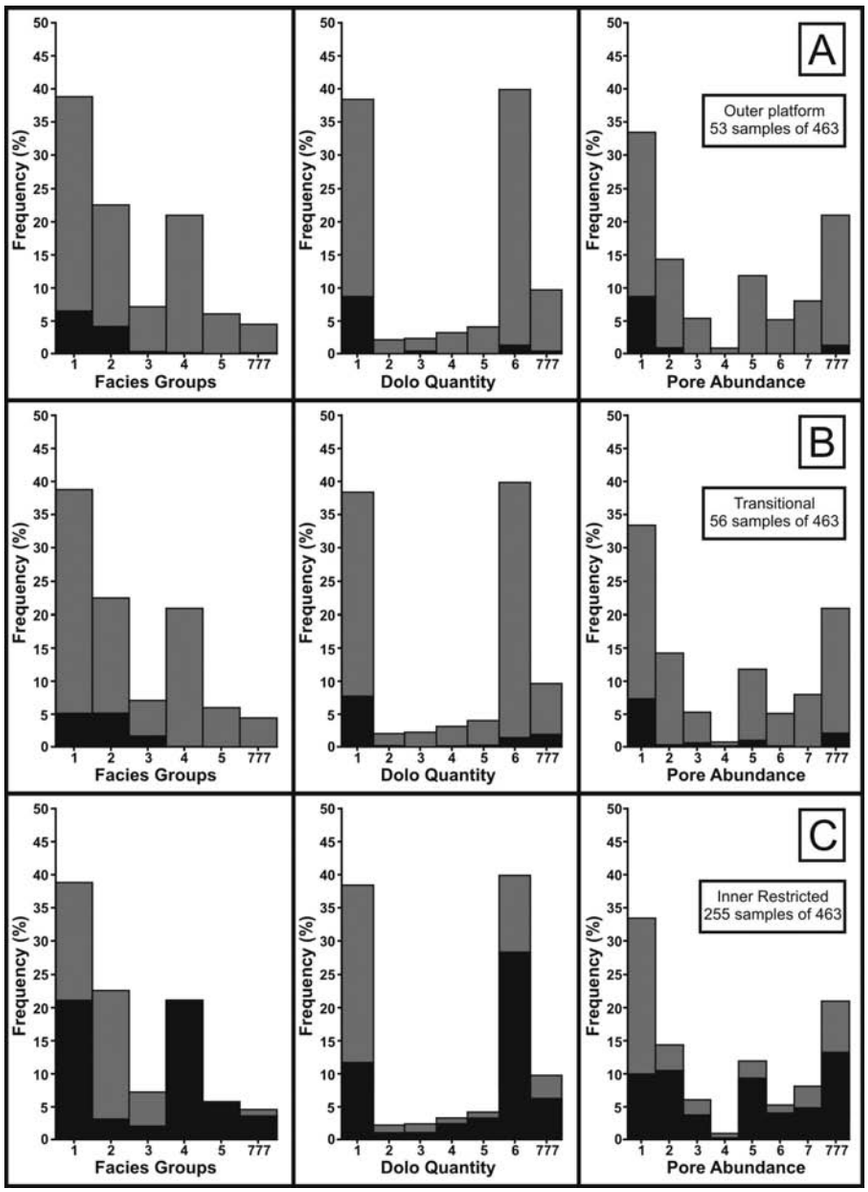

FIG. 12.—Frequency distribution of the "Facies Groups," "Dolo Quantity," and "Pore Abundance" by highlighting (in black color) samples falling in specific depositional environments. **A)** Outer platform (OP, 53 samples). **B)** Transitional outer–inner platform (T, 56 samples); **C)** Inner restricted platform (IR, 255 samples). See Table 2 for the code explanation.

dolomitized rock volume (code 6) accounts for 60% of the total. Here the pore abundance shows a more complex distribution: "absent" and "rare" classes (codes 1 and 2) account for about 38%, "rare to common" and "common" classes (codes 3 and 5) account for 26%, whereas "common to abundant" and "abundant" classes (codes 6 and 7) account for about 20%. Finally, in Stage 3 (Fig. 11C), the most represented environments are IR (code 3) and IO (code 4), with 38% of the total rock volume fully dolomitized (code 6). The pore abundance is distributed as follows: "absent" and "rare" classes (codes 1 and 2) account for about 48% and "rare to common" and "common" classes (codes 3 and 5) account for about 15%, whereas "common to abundant" and "abundant" classes (codes 6 and 7) account for less than 15%.

The statistical analysis was also performed to evaluate the abundance of dolomite ("Dolo Quantity") and type of facies ("Facies Groups") in each depositional environment (Figs. 12, 13).

It turns out that in the OP environment only 11% of the rock volume is fully dolomitized (Fig. 12A). Here the dominant facies groups are the muddy and fine grained ones (codes 1 and 2), with locally high proportions of marlstone.

The T environment contains 13% of fully dolomitized rocks (Fig. 12B). The most common facies groups are the muddy and the fine

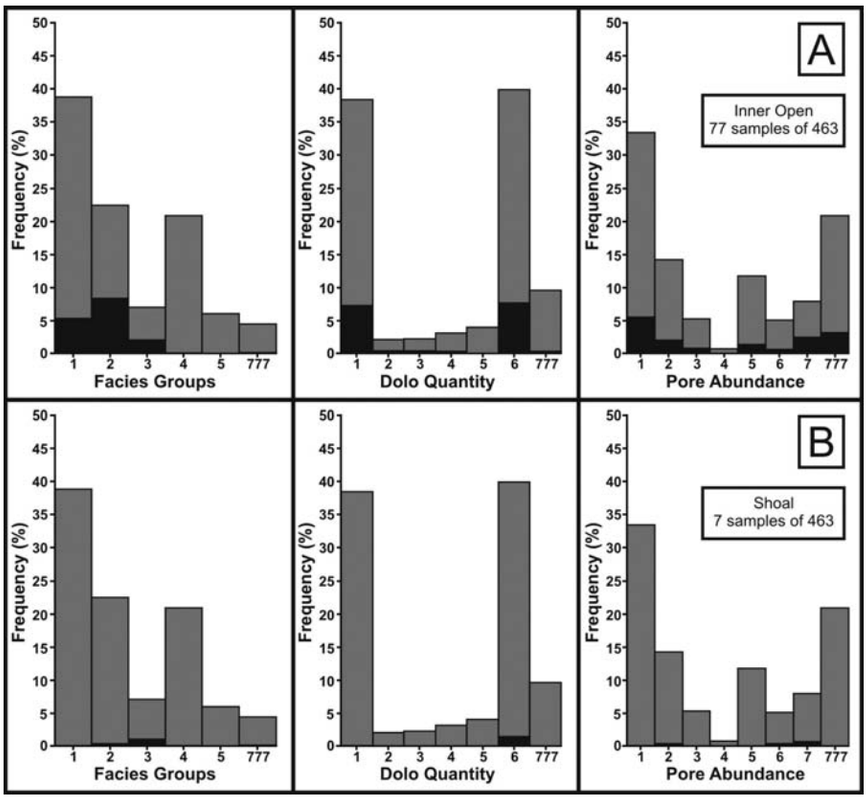

FIG. 13.—Frequency distribution of the "Facies Groups," "Dolo Quantity," and "Pore Abundance" by highlighting (in black color) samples falling in specific depositional environments. **A)** Inner open platform (IO, 77 samples); **B)** Shoal (S, 7 samples). See Table 2 for the code explanation.

grained types (codes 1 and 2). Deposits from this environment only occur during Stage 1 of platform evolution (Fig. 10).

The IR boasts with more than 50% of the rock volume being fully dolomitized and around 22% being undolomitized (Fig. 12C). This environment is mainly composed of rudist-rich (or bearing) facies and muddy facies (codes 4 and 1).

The IO lithologies are dominantly (47%) fully dolomitized, whereas 42% are not dolomitized (Fig. 13A). This environment consists mainly of fine and medium-coarse grained facies (codes 2 and 3), followed by muddy facies (code 1).

Finally, lithologies deposited in the S environment, which represent only a limited rock volume, are always (100%) fully dolomitized and are given only by fine and medium-coarse grained facies (Fig. 13B). Deposits from this environment only occur during Stage 2 of the platform evolution (Fig. 10).

The abundance of pores ("Pore Abundance") is directly proportional to the degree of dolomitization ("Dolo Quantity") in the succession. Indeed, pores mainly fall into the classes "absent" and "rare" (codes 1 and 2) in the undolomitized succession (where dolomite is absent or less than 10%) corresponding to D1 (Fig. 14A). In the partially dolomitized succession (where dolomite is in the range of 10–75%), corresponding to D2 (Fig. 14B), pores of the "absent" and "rare" classes (codes 1 and 2) are still dominant, although pores in the "rare to common" and "common" classes (codes 3 and 5) also become important, with only minor pores in the "common to abundant" and "abundant" classes (codes 6 and 7). Finally, in the fully dolomitized lithologies (where dolomite is between 75 and 100%), corresponding to D3 (Fig. 14C), pores are dominantly falling into the "common to abundant" and "abundant" classes (codes 6 and 7) and secondarily into the "rare" class (code 2).

Interdependence also exists between degree of dolomitization ("Dolo Quantity") and pore abundance ("Pore Abundance") within the different types of facies ("Facies Groups"). In particular, muddy and fine grained facies (codes 1 and 2) are mainly undolomitized and are dominated by pores falling into the classes "absent" to "rare" (codes 1 and 2; Fig. 15A). On the other hand, medium-coarse grained facies and rudist-rich (or bearing) facies (codes 3 and 4) are mainly fully dolomitized and are characterized by more abundant pores (codes 5, 6, and 7; Fig. 15B).

The main conclusions deduced from the statistical data treatment are that:

1. Dolomitization is preferentially concentrated in Stage 2 of the platform evolution, where 60% of the succession is dolomitized (Fig. 11B);
2. The most dolomitized environments correspond to the IR and the S environments, followed in importance by the IO environment (Figs. 12, 13);
3. Rudist-rich (or bearing) facies, corresponding to textures ranging from floatstone to rudstone to boundstone, are more commonly dolomitized (Fig. 15); and
4. Macroscopic porosity shows a direct proportionality with the degree of dolomitization and seems to be facies controlled: pores are more abundant in fully dolomitized portions of the succession

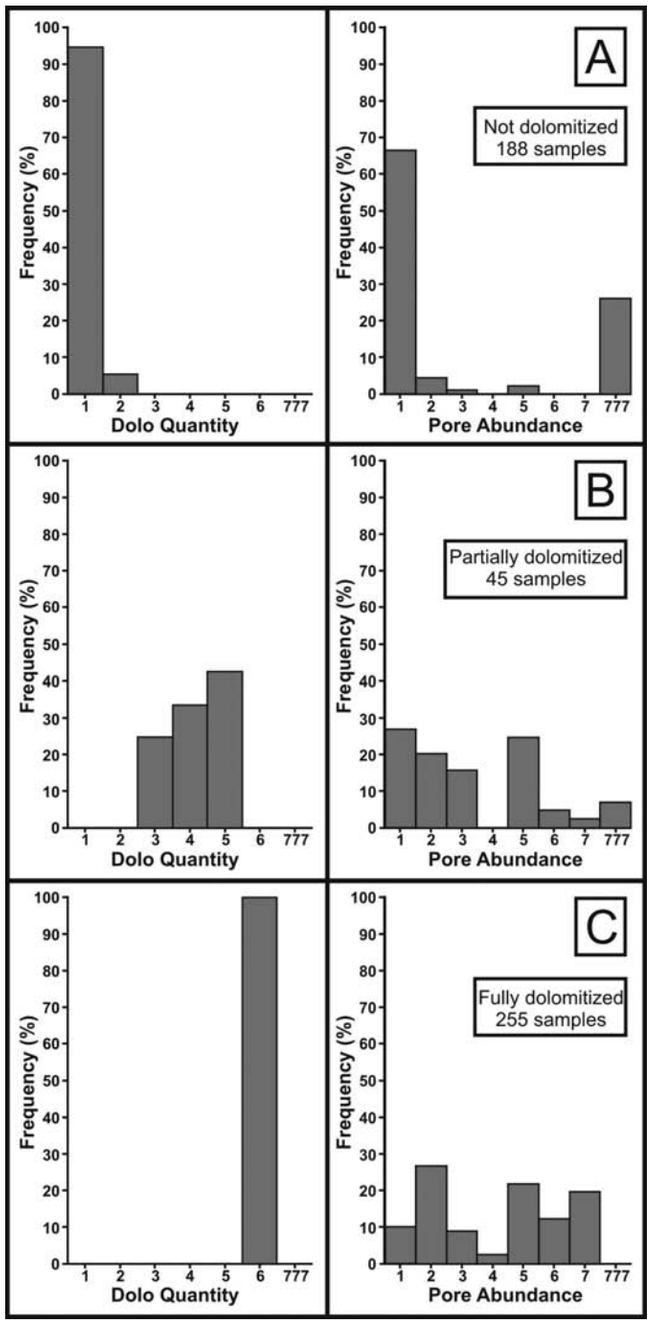

FIG. 14.—Frequency distribution of the "Pore Abundance" for different "Dolo Quantity". **A)** Not dolomitized (D1, 188 samples). **B)** Partially dolomitized (D2, 45 samples). **C)** Fully dolomitized (D3, 255 samples). See Table 2 for the code explanation.

(Fig. 14) and particularly in the rudist-rich and the medium-coarse grained facies (Fig. 15).

For the following modeling purposes, several association rules have been obtained from statistical analysis in order to summarize quantitative information that allow us to associate to each depositional environment, in each of the three platform stages, different proportions of dolomitization and related pore abundance. Tables of association rules were constructed (Table 3).

The left part of Table 3 shows the quantitative relationship (in percentages) between the depositional environments (OP, T, IR, IO, and S) and the degree of dolomitization (D1, D2, and D3) for each stage of the platform evolution (Stages 1, 2, and 3). For instance, rocks from the OP in Stage 3 of the succession are fully dolomitized (D3), partially dolomitized (D2), and undolomitized (D1) in the respective amounts of 33%, 22%, and 45%.

The right part of Table 3 illustrates the distribution of the five pore abundance classes (Φ_1, Φ_2, $\Phi_{3,4}$, $\Phi_{5,6}$, and Φ_7) in each "Environment–Dolo Quantity" couple previously established (see left part of Table 3), for each stage of the platform (Stages 1, 2, and 3). For instance, rocks from the OP of Stage 3 will always display (100%) absence of pores (Φ_1) when they are undolomitized (D1) or partially dolomitized (D2). On the contrary, when these rocks are fully dolomitized (D3), 33.3% of them will be characterized by absent pores (Φ_1), 33.3% by rare pores (Φ_2), and 33.3% by rare to common pores ($\Phi_{3,4}$).

The overall information from statistical analysis was used to establish the methodology for the geostatistical simulations (nested properties) and to obtain quantitative parameters (proportions and probabilities) with which to run the algorithms.

RESULTS OF GEOSTATISTICAL MODELING

The final objective of the geostatistical modeling is to populate a 3D grid representing the studied geological reservoir with petrophysical properties (porosities in this study), the values for which vary spatially. Prediction of the distribution of depositional facies and/or facies associations is based on hard data (wells, seismic), but also takes into account the conceptual geological model (paleoenvironmental maps, structural heterogeneities, stratigraphy, etc.). The subsurface geologist can also infer some sedimentological information from outcrop analogs (e.g., Koehrer et al. 2010). This is not the case for the petrophysical properties, which can be altered by diagenesis after deposition and for which distribution may be more difficult to predict. In the present study, the focus has been placed on the characterization, quantification, and simulation of dolomitization and pore abundance distribution. Facies, environments, dolomite abundance, etc., are only known at the sections and cores. Geostatistical methods are used to fill the space between the hard data, using parameters computed from these data (distributions laws, quantitative relationships between properties) via the statistical analysis previously described.

Data and Grid

The first step of the modeling approach was to build a geological grid, which represents the studied platform succession in terms of geometry and stratigraphy. Five stratigraphic units corresponding to the three evolutionary stages of the platform development and two subunits have been created to account for some differences in terms of depositional environments within Stages 1 and 2, resulting in a total of five units. The entire block size is 3200 m (X) by 4300 m (Y) by 196 m (Z), and the horizontal cell size is 50 by 50 m.

The layering of the units has been defined to represent the depositional model, and a proportional layering was chosen for all units to account for the syn-tectonic deposition of the sediments (Fig. 2).

The six wells (four field sections and two cores) have been imported into the grid with their three property logs (depositional environments defined by facies, dolomite quantity, and pore abundance) and resampled on the grid cells crossed by their trajectories (assignment of the property with the highest proportion

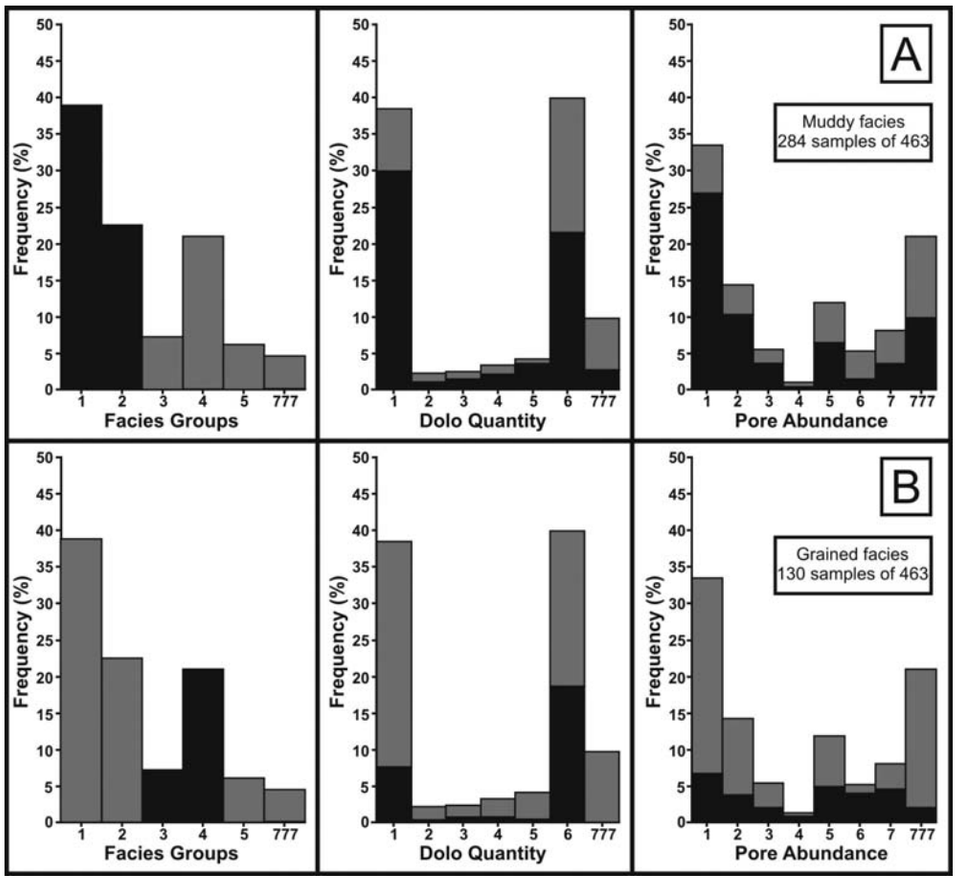

FIG. 15.—Frequency distribution of the "Facies Groups," "Dolo Quantity," and "Pore Abundance" by highlighting (in black color) samples from specific "Facies Groups." **A)** Muddy facies (code 1, 179 samples) and fine grained facies (code 2, 104 samples); **B)** Medium-coarse grained facies (code 3, 33 samples) and rudist-rich (or bearing) facies (code 4, 97 samples). See Table 2 for the code explanation.

in each cell, computed from data within the cells). Figure 16 displays the global vertical stacking of the five units painted with the proportions of depositional environment in each layer computed from the six wells (vertical proportion curve).

Plurigaussian Simulation Method and Parameters

In the proposed workflows (double-nested and bi-PGS), the geostatistical simulations of the property distribution (depositional facies, degree of dolomitization, pore abundance, etc.) on the geological grid were done using the nonstationary PGS method (Galli et al. 1994). This method allows one to take into account the lateral and vertical changes of facies, dealing with complex spatial relationships between "lithotypes," as well as to include constraints from geological information (Doligez et al. 2003, 2015; Lerat et al. 2007; Barbier et al. 2011; Hamon et al. 2015).

The main geostatistical parameters for this method are the Vertical Proportion Curves (VPC), the Matrix of Proportions (VPC Matrix), the variogram models, and the lithotype rules (similar to a facies substitution diagram; Homewood et al. 1992). The VPC represents the relative distribution of facies in the main vertical facies succession of the geological unit (Doligez et al. 1999, Ravenne et al. 2002), computed from the well facies and related to a reference paleo-horizontal surface. It also corresponds to the evolution of the proportions of each lithofacies as a function of the depth (Fig. 17), which are quantitative data needed in the PGS algorithm. In most practical cases a 3D grid of proportions is needed instead of average values at each depth to account for geological lateral changes in facies distribution. This matrix of proportions consists of a 2D grid representing a partitioning of the studied reservoir (Fig. 17), each cell being associated with a local VPC of the sedimentary facies (Armstrong et al. 2011).

In this study, the matrixes of proportion were built with the delimitation of areas assigned by VPC and geological paleoenvironmental maps defined from the geological data. An example of a paleoenvironmental map is shown in Figure 17, in which IO platform and IR platform environments are shown. The PGS simulation process consists of generating Gaussian Random Functions (GRF) using defined variogram models. The algorithm then computes in each cell of the grid truncation values of the GRF from the local proportions given by the 3D matrix of proportions to partition the field of Gaussian values and to assign a facies in each cell.

Workflow1: Double-Nested Simulations

The main steps of this workflow (presented in Fig. 6) were followed for the different units. The simulation hypotheses, parameters, and

TABLE 3.—Tables of association rules between depositional environments (OP, T, IR, IO, S), degree of dolomitization (D1, D2, D3) and macroscopic pore abundance classes (Φ_1, Φ_2, $\Phi_{3,4}$, $\Phi_{5,6}$, Φ_7) for the three stages of platform evolution (Stage 1, 2, 3). Left: Quantitative relationship between the depositional environments and the degree of dolomitization ("Environment–Dolo Quantity"). Right: Quantitative relationship between "Pore Abundance" in each of the "Environment–Dolo Quantity" couples established.

LEGEND	
Environment	**ENV**
Outer platform	OP
Transitional	T
Inner Restricted platform	IR
Inner Open platform	IO
Shoal	S
Dolomite abundance	**DOLO**
Undolomitized (0-10 % dolomite)	D1
Partially dolomitized (10-75 % dolomite)	D2
Fully dolomitized (75-100 % dolomite)	D3
Pora abundance	**Φ**
Absent	1
Rare	2
Rare to common, rare and abundant	3, 4
Common, common to abundant	5, 6
Abundant	7

(%)	DOLO	OP	T	IR	IO	S	ENV-DOLO	Φ_1	Φ_2	$\Phi_{3,4}$	$\Phi_{5,6}$	Φ_7	Total
Stage 3	D3	33	0	42	49	0	OP - D3	33,3	33,3	33,3	0	0	100
							OP - D2	100	0	0	0	0	100
							OP - D1	100	0	0	0	0	100
	D2	22	0	21	7	0	IR - D3	21	27	0	31	21	100
							IR - D2	42	25	8	17	8	100
							IR - D1	58	25	8	9	0	100
	D1	45	0	37	44	0	IO - D3	11	22	11	22	34	100
							IO - D2	80	0	0	20	0	100
							IO - D1	83	11	0	6	0	100
Stage 2	D3	17	0	64	0	100	OP - D3	0	100	0	0	0	100
							OP - D2	0	33,3	33,3	33,3	0	100
							OP - D1	100	0	0	0	0	100
	D2	50	0	17	0	0	IR - D3	5	28	13	39	15	100
							IR - D2	13,5	18	23	45,5	0	100
							IR - D1	90	10	0	0	0	100
	D1	33	0	19	0	0	S - D3	0	28	0	28	44	100
							S - D2	0	0	0	0	0	0
							S - D1	0	0	0	0	0	0
Stage 1	D3	3	15	0	0	0	OP - D3	0	0	0	100		100
							OP - D2	0	0	0	0	0	0
							OP - D1	96	4	0	0	0	100
	D2	0	8	0	0	0	T - D3	0	14	28	43	14	100
							T - D2	0	25	25	50	0	100
							T - D1	97	0	3	0	0	100
	D1	97	77	0	100	0	IO - D3	0	0	0	0	0	0
							IO - D2	0	0	0	0	0	0
							IO - D1	100	0	0	0	0	100

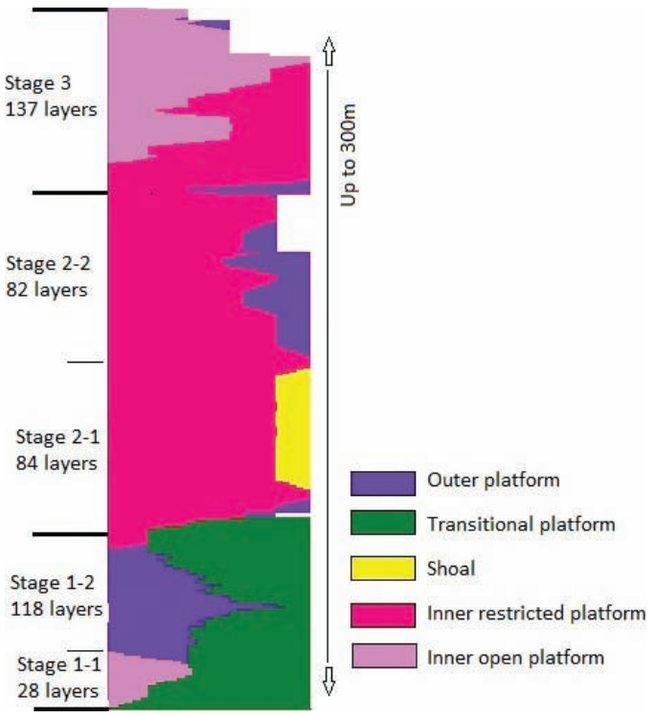

FIG. 16.—Vertical stacking of the five units and layering, painted with the proportions of depositional environment in each layer computed from the six wells (vertical proportion curve).

results of the 3D modeling of properties are presented here only for Unit 3.

Step 1: Simulation of the Distribution of Depositional Environments ("Environment"): The five depositional environments (OP, T, IO, IR, and S) have been taken into account. For each modeled unit and subunit the matrix of proportions (Fig. 17) was built based on the six VPCs of the six wells (Nieves T, Nieves B, Santa Eulalia, Duña, SC6Bis, and SC1) interpolated level by level with a kriging method and using a partition of the studied area from five paleoenvironmental maps.

Figure 18 displays one layer and one cross section in the 3D model resulting from PGS simulations of the depositional environments using two Gaussian variogram models with range values between 350 and 450 m along X direction, 500 to 700 m along Y direction, and 3 m along the vertical (Z) direction (values inferred from the continuity of the geological bodies on outcrop). Inner platform environments dominate this unit. The IR environment is located in the southwestern part of the unit, including the Duña and SC6Bis wells. The rest of the unit consists of the IO environment.

Step 2: Simulation of the Distribution of "Dolo Quantity" within "Environment": As anticipated in the "Statistical Analysis" section, the six initial classes of dolomite abundance have been merged into three classes from the six wells (D1, D2, and D3; Table 2). The dolomite abundance ("Dolo Quantity") property has been simulated from three PGSs nested in the three depositional environments ("Environment") occurring in this unit. The "Dolo Quantity" simulation parameters (proportions from Table 3, variograms, truncation rules) are specific for each depositional environment. Figure 19 displays a layer map (for level 41) and a cross section in the 3D grid after one nested simulation of the two parameters (dolomite abundance and depositional environments) performed for Unit 3. In this unit, the three represented environments are affected by the dolomitization process with close proportions (Table 3), which is what the simulation reproduced.

Step 3: Simulation of the Distribution of "Pore Abundance" Related to the Combination of "Environment–Dolo Quantity" Couples: As anticipated in the "Statistical Analysis" section, the seven initial classes of pore abundance have been merged into five classes from the six wells (Φ_1, Φ_2, $\Phi_{3,4}$, $\Phi_{5,6}$, and Φ_7; see Table 2). The results obtained from the statistical analysis (Table 3) have then been used to fix the parameters (proportions and variograms) for the simulations of the distribution of the five "Pore Abundance" classes

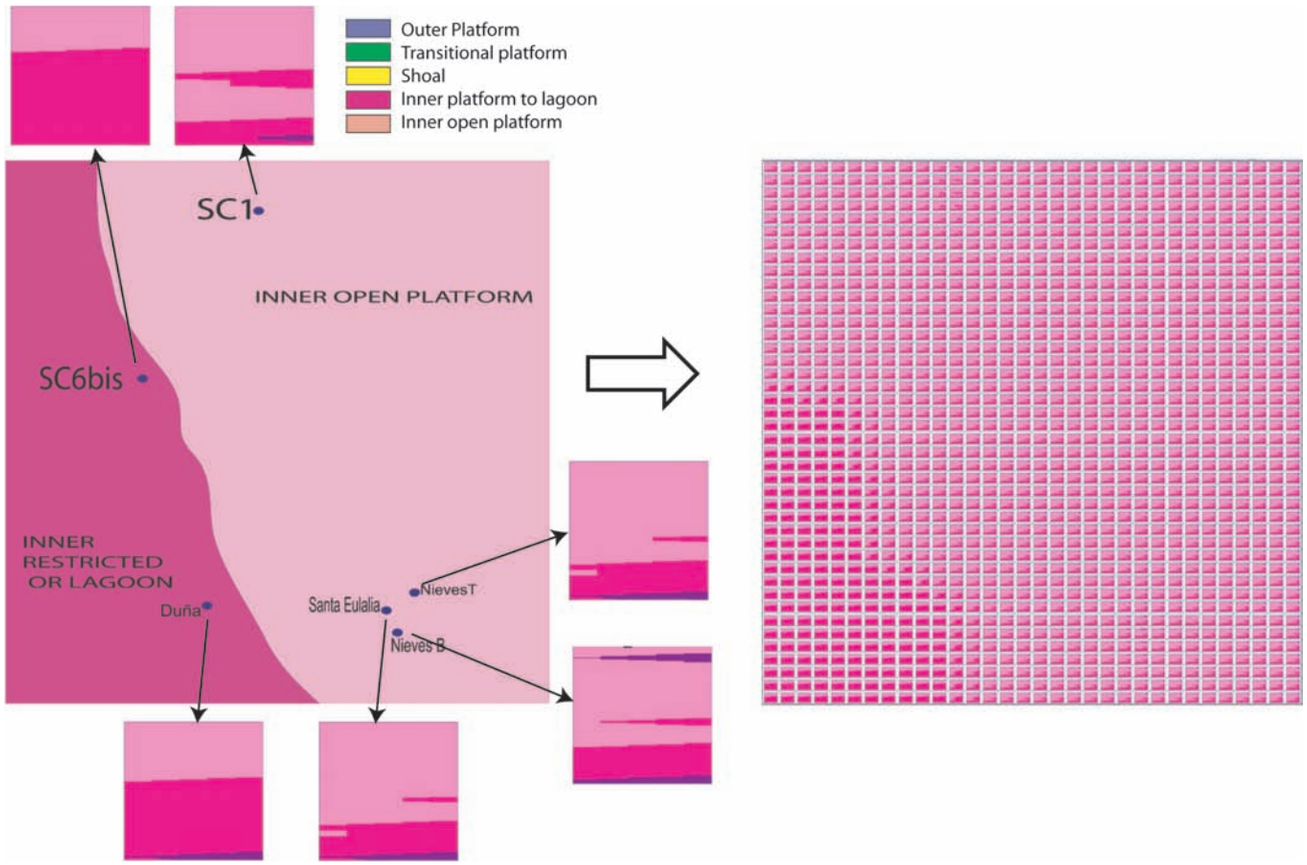

FIG. 17.—Depositional paleoenvironment map and vertical proportion curves (VPCs) for Unit 3 (left), with matrix of proportions of "Environment" (right) computed using the paleoenvironment map to partition the space. Inner platform environments (IO and IR) dominate the whole unit.

(Table 3) within each "Environment–Dolo Quantity" couple. The presented results come from a second nested approach of PGS simulation of the pore classes within the mixed property. Figure 20 displays the final grid (stacking of the five units) informed with the three properties from Workflow1 (double-nested).

Workflow2: Bi-PGS-nested Simulations

The main steps of the bi-PGS workflow (presented in Fig. 7) were followed for the different units. The simulation hypotheses, parameters, and results of the 3D modeling of properties are presented here for Unit 3.

Step 1: Computation of the Matrix of Proportions of "Dolo Quantity" from the Matrix of "Environment": In this workflow, the link between the two PGSs is given through the proportions of all the associations of one "Environment" with "Dolo Quantity" properties. This is done through the computation of the matrix of proportions of dolomite abundance from the matrix of proportions of depositional environments, using in this case the data from statistical analysis. The resulting grids of proportions are displayed in Figure 21.

Step 2: Bi-PGS Simulations of "Dolo Quantity" and "Environment": Each physical property ("Environment" and "Dolo Quantity") simulation is associated with a complete PGS, possibly using two underlying Gaussian random functions with their own variogram model, its specific truncation rule (Fig. 7), and its matrix of proportions (Fig. 21). The double nonstationary PGS simulations are processed together.

Step 3: Simulation of the Distribution of "Pore Abundance" Related to the Combination of "Environment–Dolo Quantity" Couples: At last, the simulations of the distribution of the five "Pore Abundance" classes (Φ_1, Φ_2, $\Phi_{3,4}$, $\Phi_{5,6}$, and Φ_7) within each "Environment–Dolo Quantity" couple have been performed using a nested approach. Figure 22 displays the final grid (stacking of the five units) informed with the three properties from Workflow2 (bi-PGS-nested).

DISCUSSION

This project was designed as an integrated study of a carbonate reservoir field analogue affected by widespread burial dolomitization that, according to macroscopic observations, enhanced reservoir properties of the precursor carbonates. A data set was produced from characterization of depositional facies and environments, quantification of dolomitization and pore abundance, and their statistical treatment. This multidisciplinary data set provided the basis for the

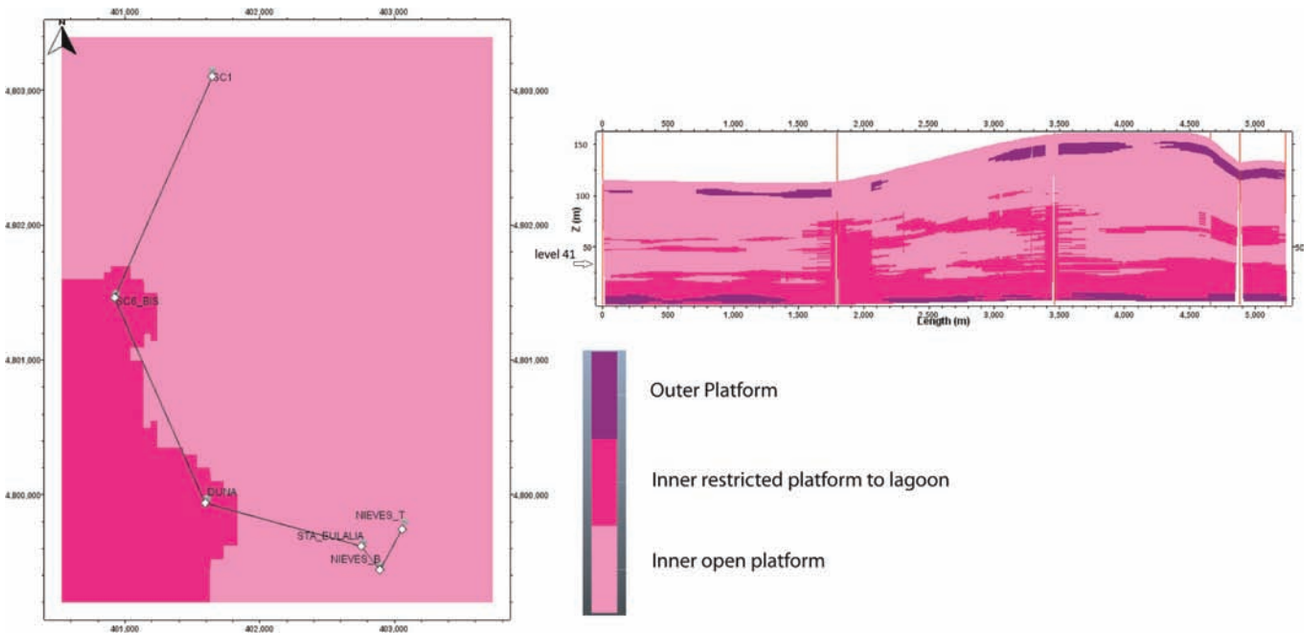

FIG. 18.—Layer map (level 41) and cross section in the 3D grid after plurigaussian simulation of one parameter ("Environment"), performed for Unit 3.

development of a quantitative reservoir study and 3D geostatistical modeling by applying different workflows.

Controls on Dolomitization and Reservoir Properties

The aim of the sedimentological, diagenetic and statistical analysis accomplished during this survey was to test at reservoir scale some hypotheses related to the controls of burial dolomitization, issued from previous conceptual studies at basin scale (López-Cilla 2009; López-Cilla et al. 2009, 2013, 2016). According to these authors, the dolomitizing fluids were channeled by regional faults through the carbonate succession during burial, and the type of precursor carbonate facies encountered by the fluids further controlled the distribution of dolomitization and the associated macroporosity. In

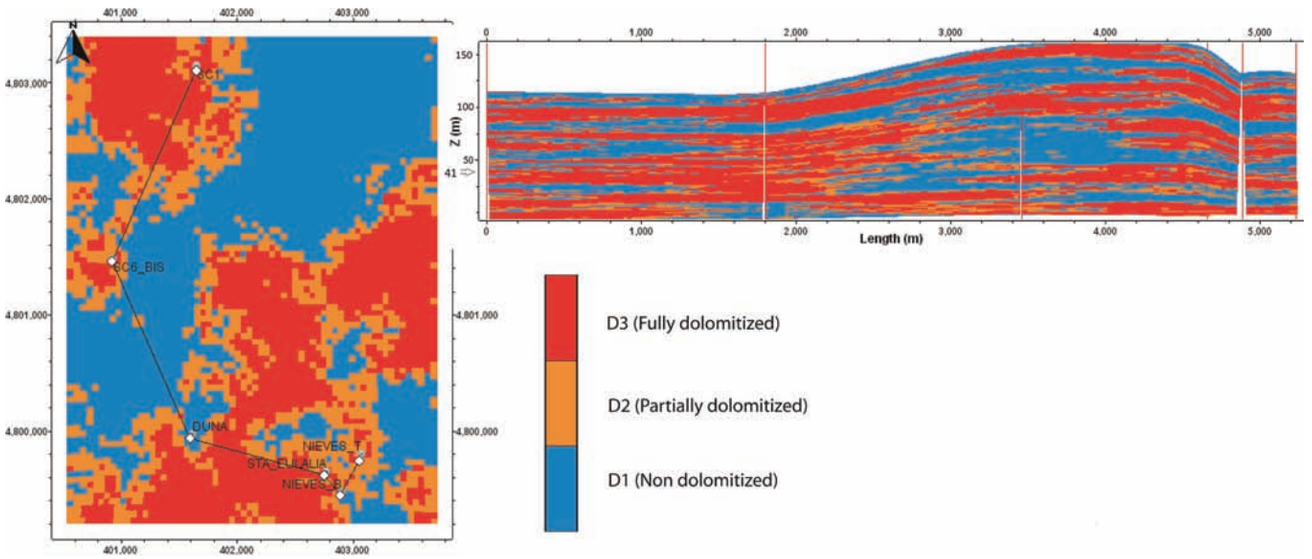

FIG. 19.—Layer map (level 41) and cross section in the 3D grid after nested simulations of the "Dolo Quantity" parameter within each "Environment," honoring the proportions defined by the statistical data analysis, performed for Unit 3.

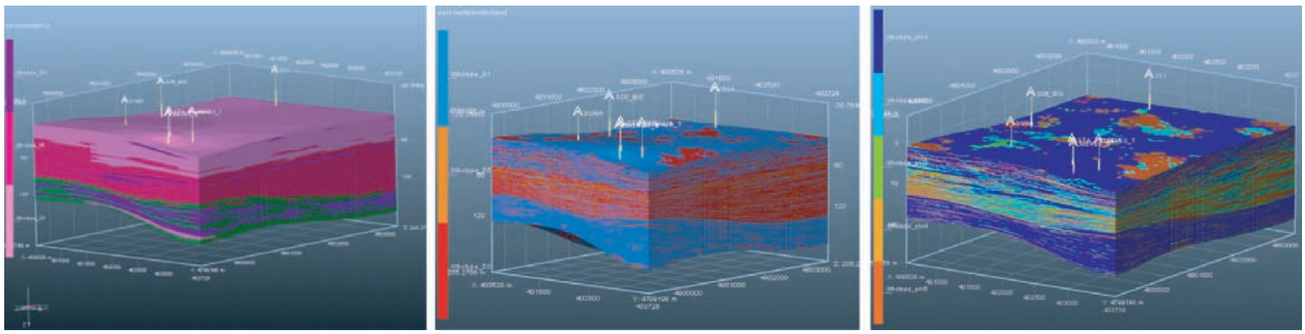

FIG. 20.—Final grid (stacking of the five units) informed with the three properties ("Environment," "Dolo Quantity," and "Pore Abundance") from the double-nested workflow for the complete succession.

particular, they suggested that dolomitization is more abundant in facies from the proximal depositional environments and that porosity is better developed in rudist- and coral-rich facies. These authors suggested a possible role played by aragonitic bioclasts, which could have been selectively affected by the early meteoric diagenesis experienced by the platform carbonates during periods of relative sea-level fall and platform subaerial exposure. Such early meteoric modification undergone by specific aragonitic shells would have controlled the development of the porosity during burial dolomitization (López-Cilla 2009; López-Cilla et al. 2009, 2013, 2016).

According to the characterization data set produced during this survey, the dolomitization is preferentially concentrated in the regressive part of the first depositional sequence of the Reocín Fm. (T–R Sequence 1) and the earliest stage of transgression of the second depositional sequence (T–R Sequence 2) corresponding with the second stage of the platform evolution (Fig. 11). It seems to be controlled by the facies associations (corresponding to paleoenvironments) and the original depositional textures: the most dolomitized facies are encountered in the inner-restricted platform with marginal shoals, followed by the inner open platform (Figs. 12, 13). Facies from these shallower and more proximal depositional environments were indeed more exposed to early meteoric diagenesis.

At basin scale, the pore abundance of the Reocín Fm. carbonates is variable and was reported to be higher in the dolomitic bodies than in the precursor limestone facies, which are predominantly tight and only rarely exhibit open voids (López-Cilla 2009, Blázquez-Fernández 2013). At reservoir scale, the dolomite bodies studied during this survey exhibit a wide range of macroscopic pore abundance, with pore types classified as intercrystalline, moldic, and vuggy. Macroscopic voids have sizes that range from submillimetric up to several centimeters (Fig. 8). The visual evaluation of the macroscopic pores allowed the definition of seven pore abundance classes (grouped in five classes in the geostatistical modeling), from absent to abundant (Table 2). Statistical analysis indicated that, in a general way, total macroscopic porosity is directly proportional to the degree of dolomitization (Fig. 14). Further relationships were observed between different carbonate textures (facies groups) and the abundance of macroscopic pores (Fig. 15), with the rudist-rich facies (dolo-floatstone and dolo-rudstone) and the sand shoals (dolo-grainstone and dolo-packstone) showing the highest pore occurrence. Abundant aragonitic shells (rudists, corals), easily leached or recrystallized during early diagenesis, could justify the higher moldic porosity in these facies.

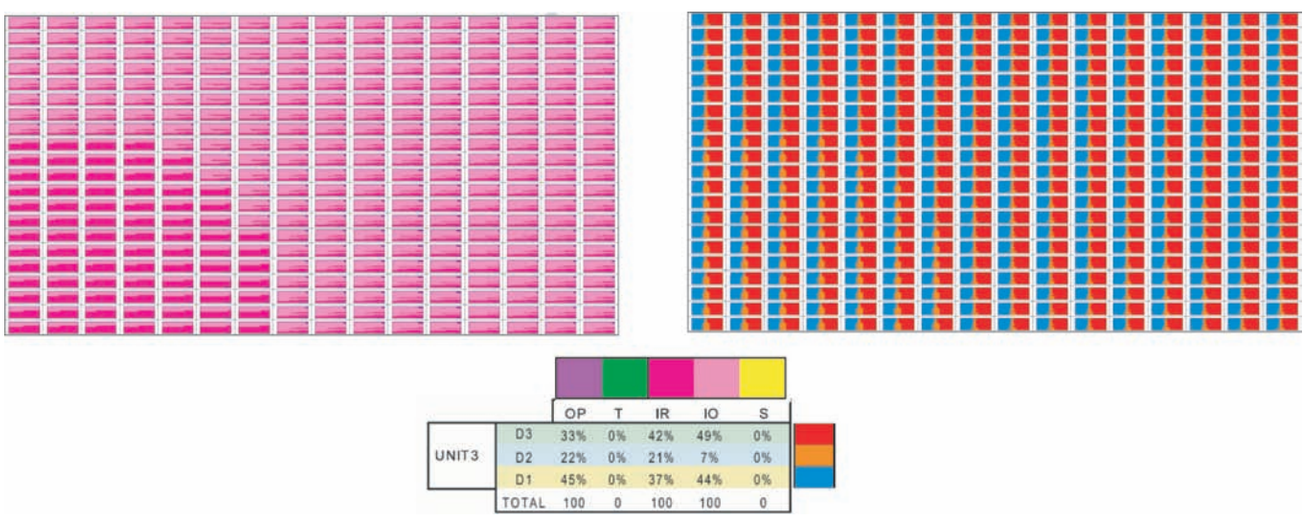

FIG. 21.—Computation of the matrix of proportions of "Dolo Quantity" from the matrix of "Environment."

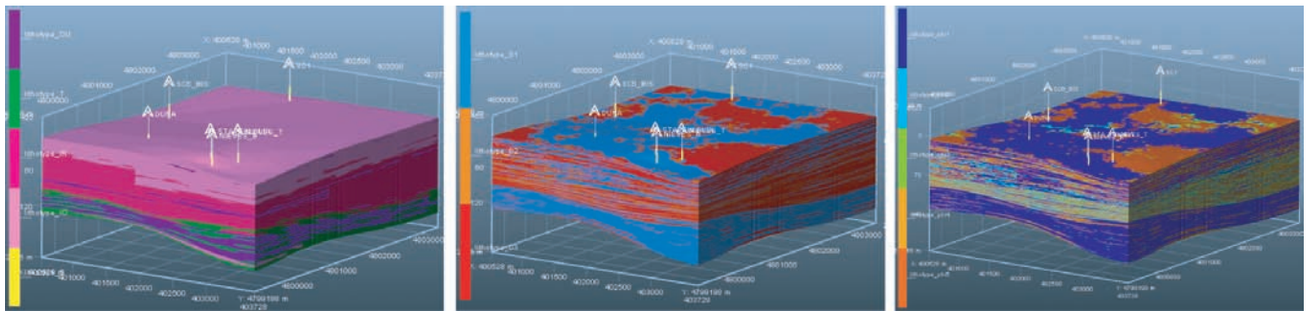

FIG. 22.—Final grid (stacking of the five units) informed with the three properties ("Environment," "Dolo Quantity," and "Pore Abundance") from the bi-PGS-nested workflow for the complete succession.

At the present stage it is not possible to say which modification the early diagenesis really caused (preferential dissolution or recrystallization of the aragonitic shell portions only?) in these facies to facilitate the development of porosity during burial dolomitization. However, this hypothesis deserves to be further investigated, since subsurface reservoirs in Urgonian-type platforms elsewhere could display similar porosity patterns. Future perspectives for this survey would therefore include applying and possibly validating the formulated hypothesis on a subsurface reservoir case study, in which detailed petrophysical measurements could also be accomplished.

3D Modeling

In carbonate reservoirs, heterogeneity is usually driven by the interplay of both depositional environments and diagenetic patterns (i.e., Morrow and MacIlreath 1990, Moore 2001, Ali et al. 2010). In this survey, characterization data from the sedimentology and diagenesis study (facies, environments, dolomitization, pore abundance) were translated into quantitative parameters and rules to distribute simultaneously the different classes of properties ("Environment," "Dolo Quantity," "Pore Abundance") in the numerical models.

In particular, this study proposed an innovative strategy, allowing us to integrate conceptual sedimentological models through the use of paleoenvironmental maps in the computation of depositional environment ("Environment") probability distribution. Moreover, a realistic 3D sedimentary model and associated diagenetic overprints have been generated through simulation of the distribution of only one diagenetic modification (e.g., the massive dolomitization ["Dolo Quantity"]), which mainly controls porosity enhancement (López-Cilla et al. 2016). Finally, petrophysical property distribution (e.g., the macroporosity ["Pore Abundance"]) has been constrained and simulated with the combination of the double property given by the "Environment–Dolo Quantity" couples.

The two alternative workflows used (double-nested and bi-PGS) allowed us to simulate the distribution of properties by taking into account different parameters. Both methods illustrate the distribution of dolomitization and pore abundance as a function of the distribution of the precursor depositional facies, which in turn are linked to the evolution of the depositional environments and relative sea-level changes.

The presented 3D reservoir models account for the thickening toward the north (cores area) and thinning toward the south (outcrops area) of the dolomitized succession. This kind of dolomitization "gradient" from north to south (Figs. 20, 22) fits with evidence for dolomite body mapping and with the proximity of the cores area to the major regional Bustriguado–Peña Castillo fault system (Fig. 2), which could have controlled the initial flush of the dolomitizing fluids through the carbonate succession.

The overall results of the workflows used are the distribution of the property "Pore Abundance" (Φ) controlled by the "Dolo Quantity" and by the "Environment" (Figs. 20, 22). The final models show that Φ_1 (absent pores) is the main class of porosity in the whole reservoir. Unit 1 is dominantly represented by Φ_1. Unit 2 is mainly represented by $\Phi_{3,4}$ (rare to common pores), with intercalations of other Φ classes. Unit 3 is represented by Φ_1 in the southeastern part of the study area and by $\Phi_{5,6}$ (common to abundant pores) and Φ_7 (abundant pores) in the remaining areas. The models also reproduce the higher pore abundance to the north and in the stratigraphic central part of the geological model, which also correspond with the most dolomitized platform areas.

The two workflows used lead to very similar results, which is to be expected, as the input data are the same for both approaches and as the same parameters (grids of proportions, variograms, truncation rules, etc.) were used for the geostatistical simulations. However, each workflow has its benefits and drawbacks and could be more appropriate than the other, depending on the geological data available and the objectives of the survey. When using a double-nested approach a high number of variables is requested, which can be laborious for practical use. A first set of parameters for the first PGS of the first property (here depositional environment) is needed. Then a second set of parameters for the second property distribution has to be defined for each class of depositional environment. On the other hand, it offers significant flexibility linked to these possible choices of parameters for the simulations. The bi-PGS workflow allows one to work with heterotopic data (when the second property is not present in each sample for which the first property is known), and it also allows one to maintain the continuity of each variable, though the definition of the relationships between the parameters to co-simulate is the most critical step of this approach. The main purpose of the study was to focus on workflows and methods by which to integrate quantitatively the diagenetic overprint in the sedimentary model. In a subsurface field case modeling study, multiple realizations and sensitivity analyses to uncertain parameters should have been carried out.

Both modeling approaches presented in this contribution require a preliminary step of characterization of prime importance. Acquisition, analysis, and interpretation of relevant data to define sedimentary facies, diagenesis, and petrophysical properties should be planned to identify and quantify their distributions and dominant relationships. Keeping in mind the opportunity to use advanced methods, such as nested or bi-PGS, should dictate the characterization workflow since the beginning of the study in order to improve the predictability of the model.

CONCLUSIONS

This study contributes to the need to develop modeling approaches that take into account the interplay between depositional-sedimentary features and subsequent diagenetic modifications in order to better and more realistically distribute the heterogeneities in carbonate reservoirs. It focused on a field analogue, which consists of an Early Cretaceous shallow-water carbonate platform in the Basque–Cantabrian basin, where widespread burial dolomitization took place. The workflow used (Fig. 1) includes field and subsurface data acquisition and interpretation, statistical characterization of sedimentary and diagenetic parameters, and geostatistical modeling using bi-PGS and nested simulations. The whole data set allows us to draw the following conclusions:

- Eighteen carbonate lithofacies were distinguished and grouped into four groups: muddy, fine grained, medium-coarse grained, and rudist-rich (or bearing) facies. They were associated with five depositional environments: inner restricted platform, inner open platform, shoal, transitional inner–outer platform, and outer platform.
- The succession was organized into two depositional transgressive–regressive (T–R) sequences. Three successive stages of platform evolution were distinguished, which are characterized by a different distribution of facies and depositional environments.
- An innovative methodology of diagenesis characterization and quantification has been tested to investigate main controls on the distribution of dolomitization and the effects on macroporosity.
- Massive burial dolomitization increases toward the middle of the studied succession, corresponding to the phase of regression of the first depositional sequence and the earliest phase of transgression of the second depositional sequence (second stage of the platform evolution).
- The dolomitization is controlled by the paleoenvironments and the original depositional facies: the most dolomitized are the inner-restricted platform with marginal shoals, followed by the inner open platform. Within these paleoenvironments, the most dolomitized lithofacies are rudist-rich floatstone, rudstone, and boundstone and sand shoals grainstone.
- Pores are most abundant in fully dolomitized portions of the succession and particularly in the medium-coarse grained and rudist-rich (or bearing) lithofacies. Abundant aragonitic shells, easily leached or recrystallized during early diagenesis, could justify the preferential development of porosity in these facies during later dolomitization.
- Two different geostatistical modeling workflows were developed using bi-PGS and nested approaches to simulate the interdependence between original depositional facies, degree of dolomitization (i.e., amount of dolomite), and pore abundance.
- The two simulation workflows lead to similar results. These methods require advanced quantitative characterization of the different classes of properties but also offer a high level of flexibility and possibilities of constraints for the simulations.
- Each workflow could be more appropriate than another depending on the geological data available and the aim of the survey.
- Future perspectives should include the application of these workflows to subsurface reservoirs, for which detailed petrophysical and production data are available, in order to evaluate to what extent the quality of reservoir modeling is affected by integrating (or not) the effects of diagenesis.

ACKNOWLEDGMENTS

The IGME is thanked for access to mine cores. This is a contribution to the research projects CGL2014-53548-P and CGL2014-54180-P (MINECO, Spanish Government). The FPU program (Ministerio de Educación, Cultura y Deporte, Spanish Government) is thanked for sponsoring the PhD Thesis of I. López-Cilla (IGME). Elisabeth Bemer (IFPEN), head of the "fluid–rock interaction" project, and Sébastien Rohais (IFPEN), head of the "CobraFlow" project, are thanked for supporting this study and the internships of S. Blázquez-Fernández and I. López-Cilla at IFPEN.

REFERENCES

Ali SA, Clark WJ, Moore WR, Dribus JR. 2010. Diagenesis and reservoir quality. *Oilfield Review* 22:14–27.

Armstrong M, Galli A, Beucher H, Le Loc'h G, Renard D, Doligez B, Eschard R, Geffroy F. 2011. *Plurigaussian Simulations in Geosciences*: Springer-Verlag, Berlin. 165 p. DOI:10.1007/978-3-642-19607-2

Barbier M, Hamon Y, Doligez B, Callot J-P, Floquet M, Daniel J-M. 2011. Stochastic joint simulation of facies and diagenesis: A case study on early diagenesis of the Madison Formation (Wyoming, USA). *Oil and Gas Science and Technology* 67:123–145. DOI:10.2516/ogst/2011009

Blázquez-Fernández S. 2013. 3D modeling of reservoir quality and prediction of a partially dolomitized carbonate platform (Basque-Cantabrian Basin, Spain) [MS thesis]: Universidad Complutense de Madrid, 55 p.

Bover-Arnal T, Salas R, Martín-Closas C, Schalagintweitt F, Moreno-Bedmar J. 2011. Expression of an Oceanic Anoxic Event in a neritic setting: Lower Aptian coral rubble deposits from the western Maestrat basin (Iberian Chain, Spain). *Palaios* 26:18–32.

Bustillo M, Ordoñez S. 1995. Lower Cretaceous Pb-Zn ores of Cantabria, northern Spain: New considerations based on petrological and geochemical evidence. *Transactions of the Institution of Mining and Metallurgy, Section B: Applied Earth Science* 104:55–65.

Choquette PW, Pray LC. 1970. Geologic nomenclature and classification of porosity in sedimentary carbonates. *American Association of Petroleum Geology Bulletin* 62:207–250.

Doligez B, Beucher H, Geffroy F, Eschard R. 1999. Integrated reservoir characterisation: Improvement in heterogeneous stochastic reservoir modeling by integration of additional external constraints. *In* Schatzinger R, Jordans J (Editors). *Reservoir Characterization—Recent Advances*, Memoir 71: American Association of Petroleum Geologists, Tulsa, Oklahoma. p. 333–342.

Doligez B, Beucher H, Pontiggia M, Ortenzi A, Mariani A. 2009. Comparison of methodologies and geostatistical approaches for diagenesis quantification. *In AAPG Annual Convention*; June 7–10, 2009; Denver, Colorado.

Doligez B, Hamon Y, Barbier M, Nader F, Lerat O, Beucher H. 2011. *Advanced Workflows for Joint Modeling of Sedimentary Facies and Diagenetic Overprint. Impact on Reservoir Quality*, SPE Paper SPE-146621: SPE Annual Technical Conference and Exhibition, Denver, Colorado.

Doligez B, Le Ravalec M, Bouquet S, Adelinet M. 2015. A review of three geostatistical techniques for realistic geological reservoir modeling integrating multi-scale data. *Bulletin of Canadian Petroleum Geology* 63(4):277–286.

Doligez B, Perrine G, Benoit G, Fournier F, Beucher H. 2003. Use of seismic to constrain geostatistical reservoir models: A quantitative approach using proportions of facies; *AAPG Annual Meeting*; May 11–14, 2003; Salt Lake, Utah.

Dunham RJ. 1962. Classification of carbonate rocks according to depositional texture. *In* Ham WE (Editor). *Classification of Carbonate Rocks—A Symposium*, Memoir 1: American Association of Petroleum Geologists, Tulsa, Oklahoma. p. 108–121.

Embry AF. 1993. Transgressive–regressive sequence analysis of the Jurassic succession of the Sverdrup Basin, Canadian Artic Archipelago. *Canadian Journal of Earth Sciences* 30:301–320.

Galli A, Beucher H. 1997. Stochastic models for reservoir characterization: a user-friendly review; *Latin American and Caribbean Petroleum Engineering Conference*; August 30–September 3, 1997; Society of Petroleum Engineers, Richardson, Texas: DOI:10.2118/38999-MS

Galli A, Beucher H, Le Loc'h G, Doligez B, Group H. 1994. The pros and cons of the truncated Gaussian method. *In* Armstrong M, Dowd PA (Editors).

Geostatistical Simulations: Kluwer Academic Publishers, The Netherlands. p. 217–233.

García-Mondéjar J. 1982. Aptiense y Albiense. Región Vasco-Cantábrica y Pirineo navarro. *In* García A (Editor). *El Cretácico de España*: Universidad Complutense de Madrid, Spain. p. 63–76.

García-Mondéjar J. 1990. The Aptian–Albian carbonate episode of the Basque–Cantabrian basin (northern Spain): General characteristics, controls and evolution. *In* Tucker ME, Wilson JL, Crevello PD, Sarg JF, Read JF (Editors). *Carbonate Platforms: Facies, Sequences and Evolution*, International Association of Sedimentologists Special Publication 9: Blackwell, Oxford, UK. p. 257–290.

Gasparrini M, Blázquez-Fernández S, Lopez-Cilla I, Rosales I, Lerat O, Doligez B, Martín-Chivelet J. 2015. A multidisciplinary modeling workflow to assess facies-dolomitization-porosity interdependence in a dolomitized Lower Cretaceous platform (northern Spain); *Advances in Characterization and Modeling of Complex Carbonates Reservoirs—1st Mountjoy Meeting*.;Abstracts Volume, Banff, Canada. p. 32.

Hamdan ARA, Alsharhan AS. 1991. Palaeoenvironments and palaeoecology of the rudists in the Shuaiba Formation (Aptian), United Arab Emirates. *Journal of African Earth Sciences* 11:569–581.

Hamon Y, Deschamps R, Joseph P, Doligez B, Schmitz J. 2015. Integrated workflow for characterizing and modeling a mixed sedimentary system: The Ilerdian Alveolina Limestone Formation (Graus–Tremp Basin, Spain). *Comptes Rendus Geosciences,* DOI:GEOSCIENCE-D-15-00090R1.

Hines FM. 1985. Sedimentation and tectonics in north-west Santander. *In* Milá MD, Rosell J (Editors). *Sixth European Regional Meeting, Excursion Guidebook*: International Association of Sedimentologists, Lleida, Spain. p. 371–398.

Homewood P, Guillocheau F, Eschard R, Cross TA. 1992. Corrélations haute résolution et stratigraphie génétique: une démarche intégrée. *Bulletin des Centres de Recherches Exploration-Production Elf-Aquitaine* 16(2):357–381.

Huck S, Rameil N, Korbar T, Heimhofer U, Wieczorek TD, Immenhauser A. 2010. Latitudinally different responses of Tethyan shoal-water carbonate systems to the Early Aptian oceanic anoxic event (OAE 1a). *Sedimentology* 57:1585–1614.

Immenhauser A, Hillgärtner H, Bentum E. 2005. Microbial-foraminiferal episodes in the Early Aptian of the southern Tethyan margin: Ecological significance and possible relation to oceanic anoxic event 1a. *Sedimentology* 52:77–99.

Journel AG, Isaaks EH. 1984. Conditional indicator simulation: Application to a Saskatchewan uranium deposit. *Journal of Mathematical Geology* 16(7):685–718.

Koehrer B, Heymann BSC, Prousa F, Aigner T. 2010. Multiple-scale facies and reservoir quality variations within a dolomite body: Outcrop analog study from the Middle Triassic, SW German Basin. *Marine and Petroleum Geology* 27:386–411, DOI:10.1016 /j.marpetgeo.2009.09.009

Labourdette R. 2007. 3D sedimentary modeling: Toward the integration of sedimentary heterogeneities in reservoir models [PhD thesis]: Université Montpellier 2, France.

Le Pichon X, Sibuet JC. 1971. Western extension of the boundary between European and Iberian plates during the Pyrenean orogeny. *Earth and Planetary Science Letters* 12:83–88.

Lerat O, Nivlet P, Doligez B, Lucet N, Roggero F. 2007. Construction of a stocha0stic geological model constrained by high-resolution 3D seismic data–Application to the Girassol Field, Offshore Angola. *In SPE Annual Technical Conference and Exhibition*; Anaheim, California

López-Cilla I. 2009. Estudio de las dolomias masivas del entorno de La Florida-El Soplao (NO de Cantabria), cuenca Vasco–Cantábrica [unpublished MSc thesis]: Universidad Complutense de Madrid, 52 p.

López-Cilla I, Rosales I, Gasparrini M, Martín-Chivelet J. 2013. Diagenesis of Lower Cretaceous platform carbonates from the northwestern margin of the Basque Cantabrian basin (northern Spain). *In 30th IAS Meeting of Sedimentology*; Conference Abstracts Volume; Manchester, UK.

López-Cilla I, Rosales I, Gasparrini M, Martín-Chivelet J. 2016. Caracterización y evolución de los fluidos diagenéticos que afectaron a los carbonatos del Aptiense superior del noroeste de la cuenca Vasco-Cantábrica (Fm. Reocín). *Geo-Temas* 16(1):551–554.

López-Cilla I, Rosales I, Najarro M, Martín-Chivelet J, Velasco F, Tornos F. 2009. Etapas de formación de dolomías masivas del entorno de La Florida-El Soplao, Cantabria. *Geogaceta* 47:65–68.

Machel HG. 2004. Concepts and models of dolomitization: A critical reappraisal. *In* Braithwaite CJR, Rizzi G, Darke G (Editors). *The Geometry and Petrogenesis of Dolomite Hydrocarbon Reservoirs*, Special Publication 235: Geological Society, London. p. 7–63.

Malod JA, Mauffret A. 1990. Iberian plate motions during the Mesozoic. *Tectonophysics* 184:261–278.

Martín-Chivelet J, Berástegui X, Rosales I, Vilas L, Vera JA, Caus E, Gräfe K-U, Mas R, Puig C, Segura M, Robles S, Floquet M, Quesada S, Ruiz-Ortiz PA, Fregenal-Martínez MA, Salas R, García A, Martín-Algarra A, Arias C, Meléndez M, Chacón B, Molina JM, Sanz JL, Castro JM, García-Hernández M, Carenas B, García-Hidalgo J, Gil J, Ortega F. 2002. Cretaceous. *In* Gibbons W, Moreno T (Editors). *The Geology of Spain*: Geological Society, London. p. 255–292.

Masse JP, Fenerci-Masse M. 2011. Drowning discontinuities and stratigraphic correlation in platform carbonates. The late Barremian–early Aptian record of southeast France. *Cretaceous Research* 32:659–684.

Masse JP, Philip J. 1981. Cretaceous coral rudistid buildups of France. *In* Toomey DF (Editor). *European Fossil Reef Models*, Special Publication 30: SEPM (Society for Sedimentary Geology), Tulsa, Oklahoma. p. 399–426.

Matheron G, Beucher H, de Fouquet C, Galli A, Guerillot D, Ravenne C. 1987. Conditional simulation of the geometry of Fluvio–Deltaic Reservoirs. *In SPE Annual Technical Conference*; September 27–30, 1987; Society of Petroleum Engineers, Richardson, Texas. DOI:10.2118/16753-MS

Moore CH. 2001. *Carbonate Reservoirs. Porosity Evolution and Diagenesis in a Sequence Stratigraphic Framework*, Developments in Sedimentology 55: Elsevier Science, Amsterdam. 444 p.

Morad S, Al-Aasm IS, Nader FH, Ceriani A, Gasparrini M, Mansurbeg H. 2012. Impact of diagenesis on the spatial and temporal distribution of reservoir quality in the Jurassic Arab D and C members, offshore Abu Dhabi oilfield, United Arab Emirates. *GeoArabia* 17(3):17–56.

Morrow DW, MacIlreath IA. 1990. *Diagenesis*, Geoscience Canada Reprint Series 4: Geological Association of Canada, Ottawa. 338 p.

Nader FH. 2017. Multi-scale quantitative diagenesis and impacts on heterogeneity of carbonate reservoir rocks. Advances in Oil and Gas Exploration and Production. DOI:10.1007/978-3-319-46445-9_3

Najarro M. 2015. Las plataformas carbonatadas y sistemas deltaicos del Aptiense-Albiense inferior del noroeste de Cantabria: registro de cambios paleoambientales y eventos anóxicos [PhD thesis]: Universidad Complutense de Madrid, 450 p.

Najarro M, Rosales I, Martín-Chivelet J. 2007. Evolución de la plataforma carbonatada de La Florida durante el *rifting* del Cretácico inferior (Aptiense, NO de Cantabria). *In* Bermudez DD, Najarro M, Quesada C (Editors). *II Semana de Jóvenes Investigadores del I.G.M.E.*: Instituto Geologico y Minero de España, Madrid. p. 123–128.

Najarro M, Rosales I, Moreno-Bedmar JA, De Gea GA, Barrón E, Company M, Delanoy G. 2011. High-resolution chemo- and biostratigraphic records of the Early Aptian Oceanic Anoxic Event in Cantabria (N Spain): Palaeoceanographic and palaeoclimatic implications. *Palaeogeography, Palaeoclimatology, Palaeoecology* 299:137–158.

Neuweiler F, Reitner J. 1992. Karbonatbanke mit Lithocodium aggregatum Elliott/Bacinella irregularis Radoicic–Palaobathymetrie, Palaookologi und stratigraphisches Aquivalent zu thrombolithischen Mud Mounds. *Berliner Geowissenschaftliche Abhandlungen* 3:273–293.

Olivet JL. 1996. Kinematics of the Iberian Plate. *Bulletin des Centres de Recherches Exploration–Production Elf Aquitanie* 20(1):131–195.

Pontiggia M, Ortenzi A, Ruvo L. 2010. New integrated approach for diagenesis characterization and simulation. *In North Africa Technical Conference and Exhibition*; February 14–17, 2010; Cairo, Egypt. Society of Petroleum Engineers, Richardson, Texas. DOI:10.2118/127236-MS

Rameil NS, Immenhauser A, Warrlich G, Hillgärtner H, Droste HJ. 2010. Morphological patterns of Aptian Lithocodium–Bacinella geobodies: Relation to environment and scale. *Sedimentology* 10:883–911.

Rat P. 1959. Les pays crétacés basco–cantabriques (Espagne) [thesis]: Université de Dijon Publications, 525 p.

Rat P. 1988. The Basque–Cantabrian basin between the Iberian and European plates: Some facts but still many problems. *Revista de la Sociedad Geológica de España* 1:327–348.

Ravenne C, Galli A, Doligez B, Beucher H, Eschard R. 2002. Quantification of facies relationships via proportion curves. *In* Armstrong M, Bettini C, Champigny N, Galli A, Remacre A (Editors). *Geostatistics, Rio 2000*: Kluwer Academic, Dordrecht, The Netherlands. p. 19–40.

Riding R. 1991. Calcified cyanobacteria. *In* Riding R (Editor). *Calcareous Algae and Stromatolites*: Springer, Berlin. p. 5–87.

Rosales I. 1999. Controls on carbonate-platform evolution on active fault blocks. The Lower Cretaceous Castro Urdiales platform (Aptian–Albian, Northern Spain). *Journal of Sedimentary Research* 69:447–465.

Saller AH, Henderson N. 1998. Distribution of porosity and permeability in platform dolomites: Insight from the Permian of west Texas. *American Association of Petroleum Geologists Bulletin* 82:1528–1550.

Schlagintweit F, Rosales I, Najarro M. 2016. *Glomospirella cantabrica* n. sp., and other benthic foraminifera from Lower Cretaceous Urgonian-type carbonates of Cantabria, Spain. Biostratigraphic implications. *Geologica Acta* 14(2):113–128.

Strebelle S, Cavelius C. 2014. Solving speed and memories issues in multiple-point statistics simulation program SNESIM. *Mathematical Geosciences* 46:171–186.

Sun SQ. 1995. Dolomite reservoirs: Porosity evolution and reservoir characteristics. *American Association of Petroleum Geologists Bulletin* 79:186–204.

Vail PR, Audemard F, Bowman SA, Eisner PN, Pérez-Cruz C. 1991. The stratigraphic signatures of tectonics, eustasy and sedimentology—An overview. *In* Einsele G, Ricken W, Seilacher A (Editors). *Cycles and Events in Stratigraphy*: Springer-Verlag, Berlin. p. 617–659.

Velasco F, Herrero JM, Yusta I, Alonso JA, Seebold I, Leach D. 2003. Geology and geochemistry of the Reocín Zinc-Lead deposit, Basque–Cantabrian basin, northern Spain. *Economic Geology* 98:1371–1396.

Warren J. 2000. Dolomite: Occurrence, evolution and economically important association. *Earth Science Reviews* 52:1–81.

Wilmsen M. 2000. Evolution and demise of a Mid-Cretaceous carbonate shelf; The Altamira Limestones (Cenomanian) of northern Cantabria (Spain). *Sedimentary Geology* 133(3–4):195–226.

Wilmsen M. 2005. Stratigraphy and biofacies of the Lower Aptian of Cuchía (Cantabria, northern Spain). *Journal of Iberian Geology* 31:25–275.